Models of Motor-Assisted Transport of Intracellular Particles

D. A. Smith* and R. M. Simmons†

*The Randall Centre for Molecular Mechanisms of Cell Function and †MRC Muscle and Cell Motility Unit, King's College London, Guy's Campus, London SE1 1UL, United Kingdom

ABSTRACT One-dimensional models are presented for the macroscopic intracellular transport of vesicles and organelles by molecular motors on a network of aligned intracellular filaments. A motor-coated vesicle or organelle is described as a diffusing particle binding intermittently to filaments, when it is transported at the motor velocity. Two models are treated in detail: 1) a unidirectional model, where only one kind of motor is operative and all filaments have the same polarity; and 2) a bidirectional model, in which filaments of both polarities exist (for example, a randomly polarized actin network for myosin motors) and/or particles have plus-end and minus-end motors operating on unipolar filaments (kinesin and dynein on microtubules). The unidirectional model provides net particle transport in the absence of a concentration gradient. A symmetric bidirectional model, with equal mixtures of filament polarities or plus-end and minus-end motors of the same characteristics, provides rapid transport down a concentration gradient and enhanced dispersion of particles from a point source by motor-assisted diffusion. Both models are studied in detail as a function of the diffusion constant and motor velocity of bound particles, and their rates of binding to and detachment from filaments. These models can form the basis of more realistic models for particle transport in axons, melanophores, and the dendritic arms of melanocytes, in which networks of actin filaments and microtubules coexist and motors for both types of filament are implicated.

INTRODUCTION

The aim of this paper is to provide a simple macroscopic theory of intracellular transport of cell organelles and vesicles, here termed "particles." Numerous experimental studies have established that these particles are equipped with bound motor proteins, which move them along microtubules and actin filaments (reviewed by Kelleher and Titus, 1998; Langford, 1995; Lambert et al., 1999). For example, anterograde transport of particles along microtubules in nerve axons is mediated by the motor protein kinesin (Vale et al., 1985a, b). In this system the motion of particles is not continuous, but saltatory (Adams and Bray, 1983; Allen et al., 1982; Rebhun, 1963; Weiss et al., 1986): particles are transported for distances of typically $\sim$10 μm at a more or less steady velocity of $\sim$1 $\mu m \cdot s^{-1}$, but there are pauses lasting for upward of 1 s in which a given particle is apparently undergoing Brownian motion and has presumably detached from the microtubule, or is stuck. There is apparently no published theoretical treatment of the kinetic motion of particles moving under the combined action of diffusion and motor transport, and no treatment at all for bidirectional motor transport. As a first step we have developed a "reaction-diffusion-transport" model: using simple kinetics to describe the interaction of particles with microtubules or actin filaments, and allowing free diffusion of unattached particles and steady motion of attached particles, net movement is described by partial differential equations which we have solved for a number of boundary conditions.

Unidirectional motor transport along a single filament system is the simplest case found in nature. However, motor transport along microtubules has been shown in some cases to be bidirectional, that is, particles can be transported in either direction, and individual particles sometimes appear to switch direction at random (Cooper and Smith, 1974). Bidirectional motion occurs (Schnapp et al., 1985) either because microtubules of both polarity are present, or because of the presence on the same particle of two motor proteins (kinesin and dynein) with opposite polarity (Schnapp and Reese, 1989; Schroer et al., 1989). At first sight bidirectional motor action would seem to be an ineffective mechanism for net transport, but in the presence of a concentration gradient it could nevertheless accelerate the rate of material transport compared with diffusion. There is an analogy with the process of "facilitated diffusion," in which the diffusion of a solute is aided by binding to a protein (e.g., O_2 to myoglobin), thus increasing the amount in solution (Wittenberg, 1966; Wittenberg et al., 1975; Wyman, 1966). Facilitated diffusion has also been reported for the faster-than-diffusion movement by which DNA-binding proteins find their target sequence, by hopping or sliding along the DNA (Hannon et al., 1986). We compare the results for unidirectional and bidirectional transport for a number of boundary conditions.

A further (and perhaps more general) complication in transport studies is the coexistence of a myosin-mediated transport system (Bridgman, 1999; Tabb et al., 1998; Wu et al., 1997) which transports particles along the actin cytoskeletal network (Schliwa et al., 1981). Actin-based transport is the sole system in the leading edge and filopodia of nerve growth cones (Evans and Bridgman, 1995; Cramer,

Received for publication 17 April 2000 and in final form 12 September 2000.

Address reprint requests to Dr. R. M. Simmons, The Randall Centre, New Hunt's House, King's College London, Guy's Campus, London SE1 1UL, UK. Tel.: 44-207848-6448; Fax: 44-207848-6435; E-mail: robert.simmons@kcl.ac.uk.

0006-3495/01/01/45/24 $2.00

1997 and refs. therein) and at the tips of melanocyte dendrites (Wu et al., 1998), but elsewhere actin-based transport coexists with microtubular transport. The actin cytoskeleton can be considered to be bidirectional because in general it consists of a network of cross-linked randomly polarized filaments (although there is at least one unidirectional exception in the case of *Nitella*; Sheetz and Spudich, 1983). Bidirectional particle transport on the actin network has been observed by depolymerizing the microtubules in axons (Bridgman, 1999; Morris and Hollenbeck, 1995), melanocytes (Wu et al., 1998), and melanophores (Rodionov et al., 1998; Rogers and Gelfand, 1998). We have not attempted to include actin-based and microtubule-based transport in the same model, but we show that bidirectional motor transport may reduce to a type of diffusion: in the one-dimensional case in which a particle detaches and re-attaches many times from the filament system in the period of observation, bulk movement is equivalent to diffusion with a modified diffusion constant. This is readily accommodated in our model.

Melanin-producing cells are a particularly attractive prospect for quantitative analysis and theoretical modeling. In the melanophores of fish and frogs, rapid darkening of the skin is achieved by the dispersion of pigment granules from a band near the nucleus to the cytoplasm, with pigment granules being retained in the cytoplasm by a myosin-actin filament system. The distribution of pigment can be reversed, presumably via control of the functionally active motor protein type by a signaling pathway. In mammals, the melanocyte is responsible for producing pigment granules, the melanosomes, which are transported down to the ends of dendritic processes, where they are engulfed by keratinocytes, and thus lend the skin its coloration (Jimbow and Sugiyama, 1998). Transport is again mixed: the bidirectional microtubular system transports melanosomes to the tips of dendrites, where they are captured by an actin system (Wu et al., 1998). The motor for actin-based melanosome transport is myosin V, for which motor speeds of 0.3–0.4 μm/s have been observed (Cheney et al., 1993; Evans et al., 1998; Wolenski et al., 1995; Mehta et al., 1999).

With transport in axons and dendrites particularly in mind, we have found one-dimensional solutions of a reaction-diffusion-transport model that give the flux of particles and their spatial distribution in various situations:

1. Steady-state transport of particles from the cell body along an axon or dendrite ("arm") of finite length, when the concentrations of free particles at each end of the arm are held constant. The results include several experimentally relevant boundary conditions at the tip of the arm, for example when the arm is closed and stationary or growing longitudinally, or when particles are trapped by a cold block. The problem of loading onto microtubules is considered;
2. The rise time for transporting a step increase in the concentration of particles at one end (the cell body) is also calculated as a function of the length of the arm and fitted to a formula based on random walks;
3. Dispersion of particles from their starting position within a long arm, after injection or pulse-labeling at the midpoint of a long arm, corresponding to diffusion along an infinite tube. The results also apply to particles injected or pulse-labeled at a particular location.

Some of these situations have analogs in the classical theories of diffusion or heat conduction (Carslaw and Jaeger, 1959) but, as indicated above, the phenomena are generally more complex. For example, diffusion of free particles and motor transport cannot be considered as separate pathways, except when attachments to filaments are irreversible. Although the literature suggests that cellular organelles may not diffuse readily in cytoplasm, it is important to be able to predict the contribution of free-particle diffusion for a given value of the diffusion constant D. Free diffusion adds significantly to motor transport over short distances when particles bind weakly to filaments.

In the Discussion section, the ability of these unidirectional and bidirectional models to describe specific cellular transport systems is assessed after reviewing the experimental literature, and ways are suggested of overcoming some obvious deficiencies of the models. For example, motor transport is treated phenomenologically by assuming a steady motor velocity v, which should be viewed as a constitutive coefficient for a law of active transport (flux α density of bound particles) analogous to the diffusion constant for Fick's law of free diffusion (flux α density gradient of free particles). Because the models work with particle densities, they predict only the macroscopic behavior of a large number of particles viewed as a continuous fluid moving in the cytoplasm. However, the densities as functions of position can also be interpreted as probability distributions for the location of a single particle. The meanings of mathematical symbols used in this paper are defined in Table 1.

A THEORY OF MOTOR-ASSISTED TRANSPORT

General equations

If attention is restricted to a single filament system (microtubules or actin), a macroscopic transport theory of particles can be formulated in terms of the laws of diffusion and kinetics. For simplicity, all motions are restricted to one space dimension, but generalizations to particle motions in three dimensions and two- or three-dimensional filament networks are straightforward.

The basic assumptions are 1) a "particle" consists of a complex between an organelle or vesicle and motor proteins (permanently attached to the surface membrane); 2) particles either diffuse freely in solution or move on a filament at a steady velocity v (the "motor velocity"), which may depend on the number of motors on the particle; 3) binding to and detachment from filaments are kinetic processes specified by first-order rate constants, which include factors as appropriate for lateral diffusion and the density of motor proteins and filaments; and 4) in the general case of bidirectional transport, binding is followed by motion in either direction, as a result of

TABLE 1 Glossary of mathematical symbols. Alternative formulas apply to unidirectional and bidirectional models, respectively

D	Free diffusion constant of the particle
D_*	Effective diffusion constant for free and bound motions
ε	l/l_{on}
F	Flux facilitation factor over free diffusion
$G_{ij}(x, t)$	Green's function for displacement from point source with initial and final states i, j
J	Particle flux (no/s/unit area) in the arm
$J_o(x, t)$	Flux of free particles
$J_\pm(x, t)$	Flux on $\pm$-directed filaments
k, k'	Binding/detachment rates to/from filaments of one polarity
K	Equilibrium constant with filaments of one polarity $= k/k'$
l_{off}	Mean free path length $= (D/k)^{1/2}$ or $(D/2k)^{1/2}$
l_{on}	Mean path length on a filament $= v/k'$
L	Arm length
λ, $\tilde{\lambda}$	Loading parameters for particles in cell body and tip regions
n, $\tilde{n}$	Particle concentrations in cell body and tip
$n_o(x, t)$	Free particle concentration
$n_\sigma(x, t)$	Concentration on filaments of polarity $\sigma = \pm 1$
$m(x)$, $n_1(x)$	$n_+(x) - n_-(x)$, $n_+(x) + n_-(x)$
η	l_{on}/L
$p(x, t)$	Probability of displacement x after time t
p_j,	Initial probability of particle in state j,
p	Initial bound fraction
r	Equilibrium bound fraction (duty ratio) $= K/(K + 1)$ or $2K/(2K + 1)$.
$S(t)$	Displacement variance at time t
t	Elapsed time
τ_{off}	Mean lifetimes of free particles $= 1/k$ or $1/2k$
τ_{on}	Mean lifetime of bound particles $= 1/k'$
v	Motor speed of particle on filaments
$\bar{v}$	Mean particle velocity $= rv$
x	Particle displacement or position in an arm
ξ	l_{on}/l_{off}

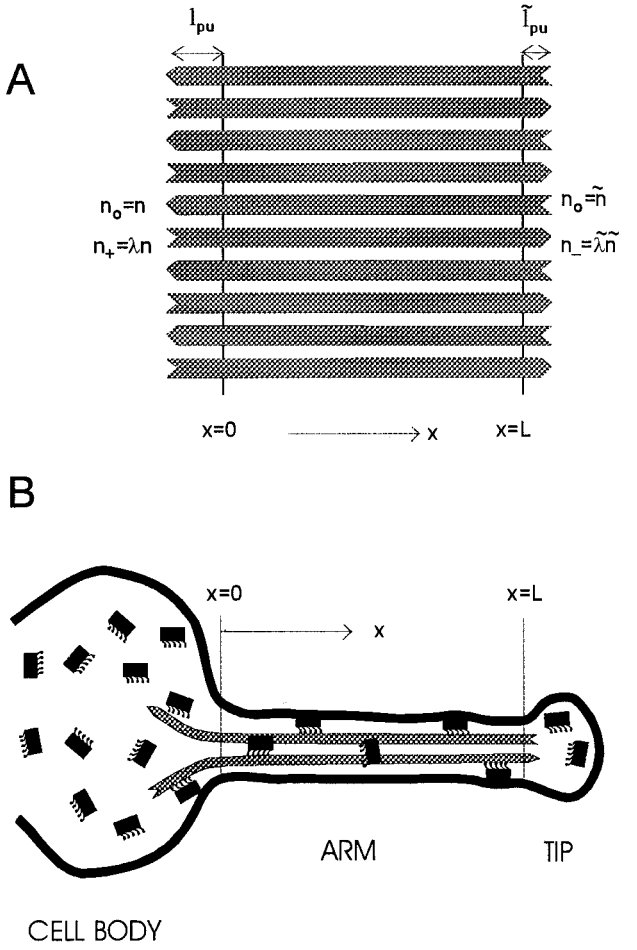

FIGURE 1 (*A*) Geometry of the one-dimensional bidirectional model. Diffusion and transport occur in a medium between planes $x = 0$ and $x = L$ at fixed temperature and pressure. A fixed fraction of this medium is filled with a homogeneous mixture of right-directed ("outward") and left-directed ("inward") filaments in known proportions, on which particles (not shown) are moved right or left by motor transport at velocities v_+, v_-. The remaining space allows diffusion of unbound particles in the x-direction, while lateral diffusion is assumed to have homogenized any lateral concentration gradients of free particles. First-order rate constants k_+, k_- determine binding to outward and inward filaments. The medium is open at $x = 0$ and $x = L$ to reservoirs of free particles at concentrations n, $\tilde{n}$. Outward filaments project into the reservoir at $x = 0$ and inward filaments into the reservoir at $x = L$ by distances l_{pu}, $\tilde{l}_{pu}$, along which "loading" of particles onto the projecting filaments occurs. (*B*) A cartoon of bidirectional particle transport in a cell "arm" (axon or dendrite), equivalent to *A*. The cell body and the tip of the arm act as reservoirs. Particle fluxes (number/second/unit area) in the arm are assumed to be axial, homogeneous throughout the arm, and equal to those obtained in *A*.

the presence of filaments and/or motors with both polarities. For convenience it is assumed that it is the polarity of the filaments that determines the direction in which particles are transported.

The one-dimensional case describes transport between two planar boundaries, say at $x = 0$ and $x = L$, all particle concentrations varying only along the x-axis (Fig. 1 *A*). A fraction of the space between the boundary planes is homogeneously occupied with filaments oriented along the x-axis. The remaining space allows diffusion of unbound particles in the x-direction. "Outward" filaments transport particles toward the right-hand end ($x = L$) and "inward" filaments toward the left-hand end ($x = 0$). All filaments are assumed to span the intervening space. This model may be interpreted as a simplified description of axial transport in an axon or cellular dendrite ("arm") between the cell body and the tip of the arm (Fig. 1 *B*), which motivates various boundary conditions at each end of the arm (discussed in the following sections). For convenience we use the terms related to the cell biology ("arm," "cell body," "tip") in most of what follows.

We first derive particle equations of motion for the most general bidirectional transport model. Let $v_+ > 0$ and $v_- < 0$ be the motor velocities in the direction of increasing x for particles traveling on outward and inward filaments, respectively. Let k_+ and k_- be the corresponding first-order rate constants for binding to filaments, and k'_+ and k'_- the rate constants for detachment. The final parameter is the diffusion constant D of the free particle.

Let $n_o(x, t)$ be the number density (per unit volume) of free particles at distance x along the arm at time t, and $n_\pm(x, t)$ the densities on right- and left-directed filaments. $n_o(x, t)$ and $n_\pm(x, t)$ satisfy reaction-diffusion-transport equations

$$\frac{\partial n_o(x, t)}{\partial t} - D\frac{\partial^2 n_o(x, t)}{\partial x^2} = -(k_+ + k_-)n_o + k'_+ n_+ + k'_- n_-, \quad (1a)$$

$$\frac{\partial n_{\pm}(x,t)}{\partial t} + v_{\pm}\frac{\partial n_{\pm}(x,t)}{\partial x} = k_{\pm}n_o - k'_{\pm}n_{\pm}. \qquad (1b)$$

The particle flux $J(x, t)$ (the number per second per unit area normal to filaments at position x) arises from diffusion of free particles and convection of bound ones, so

$$J(x,t) = J_o(x,t) + J_+(x,t) + J_-(x,t) \qquad (2a)$$

where

$$J_o(x,t) = -D\frac{\partial n_o(x,t)}{\partial x}, \quad J_{\pm}(x,t) = n_{\pm}(x,t)v_{\pm}. \qquad (2b)$$

Because $\partial(n_o + n_+ + n_-)/\partial t = -\partial J/\partial x$, J is a constant of the motion under steady-state conditions. The sign of bound-state fluxes is determined by the polarity of the filament, while the diffusion flux can be of either sign; thus particles can be exchanged between the ends of an arm even when the net flux is zero.

Motor-assisted transport can be understood in terms of mean lifetimes τ_{off}, $\tau_{\pm}$ and mean path lengths l_{off}, $l_{\pm}$ for free and bound particles, where $l_{off}^2 = D\tau_{off}$ and $l_{\pm} = |v_{\pm}|\tau_{\pm}$, so

$$\begin{aligned} \tau_{off} &= (k_+ + k_-)^{-1}, \quad & l_{off} &= \sqrt{D/(k_+ + k_-)}, \\ \tau_{\pm} &= 1/k'_{\pm}, & l_{\pm} &= |v_{\pm}|/k'_{\pm}. \end{aligned} \qquad (3)$$

The average speed $v_D = l_{off}/\tau_{off} = \sqrt{(k_+ + k_-)D}$ of free diffusion over the lifetime of the "off" state is also useful. As an example, values for a 1-μm diameter particle moving on microtubules might be $v_{\pm} = \pm 1$ μm/s, $k_{\pm} = 1\ s^{-1}$, $l_{\pm} = 10$ μm, and $D = 0.1$ $\mu m^2/s$ (Table 2), giving $l_{off} = 0.224$ μm and $v_D = 0.447$ μm/s. Binding rates reflect the density of filaments and intracellular structures may reduce the apparent value of the diffusion constant; thus this estimate for v_D may be an upper limit.

Dispersion and drift

Consider a sequence of many particle displacements, each initiated by binding to a randomly selected filament which determines the direction of motion and terminated by detachment. If free diffusion is absent and periods of detachment are negligibly small, these random walks define a form of facilitated diffusion with known mean bound path lengths $l_{\pm}$. However, this effect is generally accompanied by convection of particles at the drift velocity

$$\bar{v} = \frac{K_+v_+ + K_-v_-}{K_+ + K_- + 1}. \qquad (4a)$$

When $\bar{v} \neq 0$, motor-assisted diffusion occurs in a frame of reference moving with this velocity, with an effective diffusion constant

$$D_* = \frac{D + K_+(v_+ - \bar{v})^2/k'_+ + K_-(v_- - \bar{v})^2/k'_-}{K_+ + K_- + 1} \qquad (K_{\pm} \equiv k_{\pm}/k'_{\pm}), \qquad (4b)$$

the equilibrium average of free and bound contributions with binding constants $K_{\pm}$ for filament systems of opposite polarity. This formula is exact in the limit of many attachment cycles, even for unidirectional transport ($K_- = 0$) where all displacements are in the same direction. In this case a spread of displacements about the mean arises from variable attachment times on filaments.

TABLE 2 Derived parameters for the bidirectional model

k' (s^{-1})	K	ξ	D_*/D	τ_c (s)
5	0.2	0.089	0.72	0.7
		(0.89)	(72)	
0.5	2	0.89	0.36	2.5
		(8.9)	(36)	
0.05	20	8.9	1.98	20.5
		(89)	(198)	
0.005	200	89	19.95	200.5
		(890)	(1995)	

Derived parameters $K = k/k'$, mean path ratio $\xi = (2kv^2/Dk'^2)^{1/2} = l_{on}/l_{off}$, the ratio of compound to free diffusion constants D_*/D (Eq. 4), and the mean cycling time $\tau_c = 1/2k + 1/k'$ for the symmetric bidirectional model. The values $D = 0.1$ $\mu m^2/s$, $v = 0.1$ μm/s, and $k = 1\ s^{-1}$ define a standard set of primary parameters for numerical work. The Einstein-Stokes relation gives $D = 0.4$ $\mu m^2/s$ for a 1-μm diameter sphere in water; this value has been rounded down to allow for an irregular surface topology and a bigger cytoplasmic viscosity. Derived values for a fast motor-filament system ($v = 1$ μm/s) are shown in parentheses.

Boundary conditions, loading

To describe particle transport in a cell arm (for example, an axon or dendrite), solutions of Eqs. 1 require appropriate boundary conditions. In the first instance, let the boundaries at $x = 0$ and L be open to reservoirs of free particles at fixed concentrations n and $\tilde{n}$, respectively. Throughout, the reservoir in $x < 0$ is identified as the cell body, which is assumed to be large enough that n is constant. At the tip of the arm, the situation is more complicated and is dealt with below. If filaments in the arm do not protrude into these reservoirs, the boundary concentrations for bound particles must be zero. However, outward filaments are known to extend back into the cell body, for example under the plasma membrane (Wu et al., 1998). In that case, outward filaments emerging from the cell body are already "loaded" with particles, and the boundary value for $n_+(x, t)$ at $x = 0$ may be written as λn, where λ will be called the "degree of loading."

The tip of a cell arm is, in some cases, closed rather than open to a particle reservoir, though a store of particles in the tip can be achieved by the presence of an auxiliary filament system (Wu et al., 1998). Moreover, outward transport of particles at the tip is often associated with its physical growth, which is compatible with a closed but moving boundary. For the time being, we choose to work with fixed concentrations of free and minus-directed particles at the tip end $x = L$, giving boundary conditions

$$\begin{aligned} n_o(x=0) &= n, \quad & n_o(x=L) &= \tilde{n}, \\ n_+(x=0) &= \lambda n, \quad & n_-(x=L) &= \tilde{\lambda}\tilde{n}. \end{aligned} \qquad (5)$$

The degree of loading $\tilde{\lambda}$ in the tip may be smaller than λ or even zero. Under steady-state conditions, predictions obtained with these boundary conditions may readily be transferred to a closed tip, whether stationary or moving.

The loading coefficients may be calculated kinetically in terms of the "pick-up" lengths defined in Fig. 1. For outward filaments at $x = 0$ extending back into the reservoir by a distance l_{pu}, solving the steady-state reaction-transport equation $v_+ dn_+(x)/dx = k_+n - k'_+n_+(x)$ for $-l_{pu} < x < 0$ and $n_+(-l_{pu}) = 0$ gives $n_+(x) = K_+n\{1 - \exp(-k'_+(x + l_{pu})/v_+\}$. Hence $\lambda = K_+\{1 - \exp(-k'_+l_{pu}/v_+)\} < K_+$.

Solution of equations, scaling

Solutions of Eqs. 1 are first sought for the case of unidirectional motor transport where all particles have only one kind of active motor protein and the filaments are unipolar ($k_+ = k$, $k_- = 0$). Bidirectional motor transport, in which filaments of both polarities exist or different motors of opposite

polarity exist on the same particle, is studied here only for the symmetrical case $k_\pm = k$, $k'_\pm = k'$, and $v_\pm = \pm v$. Algebraic solutions simplify considerably when the arm is longer than the diffusion length l_{off}, which is expected and assumed throughout. For the bidirectional case, it is convenient to make separate predictions for the case when particles bind irreversibly to filaments until motor action takes them to the end. In both cases the predicted behavior is a function of the four basic parameters D, v, k, k' plus loading parameters and the length of the arm.

The required amount of computation is eased by using scaling relationships that follow from the existence of scaled dimensionless solutions. These may be obtained by choosing v/k and $1/k$ as units of length and time, which leads to a dimensionless detachment rate $1/K = k'/k$ and a dimensionless diffusion constant Dk/v^2. In this way, scaling laws for the concentrations

$$n_i(x, t|\Lambda^2 D, \Lambda v, k, k') = \Lambda^{-3} n_i\left(\frac{x}{\Lambda}, t|D, v, k, k'\right), \tag{6a}$$

$$n_i(x, t|D, \Lambda^{1/2} v, \Lambda k, \Lambda k') = \Lambda^{-3/2} n_i(\Lambda^{1/2} x, \Lambda t|D, v, k, k') \tag{6b}$$

in which the four basic parameters are displayed can be derived from Eqs. 1, where $\Lambda > 0$ is an arbitrary scaling factor and $i = 0, \pm$. Thus the number of independent parameters is reduced from four to two, say the detachment rate k' and motor velocity v, while D and k can be held fixed. This procedure is adopted throughout the paper, setting $D = 0.1\ \mu m^2/s$ and $k = 1\ s^{-1}$. Equation 6a shows that the effects of reducing the diffusion constant by a factor of $\Lambda^2 < 1$ are equivalent to those obtained by raising the motor velocity and position x along the arm by a factor of $1/\Lambda$, so computed solutions should be available for more than one motor velocity. Similarly, the effect of reducing the binding rate by a factor of Λ is equivalent to keeping the equilibrium constant K unchanged, raising the motor velocity by a factor of $\Lambda^{-1/2}$, and reducing the position coordinate by $\Lambda^{1/2}$ (Eq. 6b). Similar results follow for the net outward flux J at the tip of a cell arm. In terms of the mobility J/n,

$$\frac{J}{n}(L, t|\Lambda^2 D, \Lambda v, k, k') = \Lambda \frac{J}{n}\left(\frac{L}{\Lambda}, t|D, v, k, k'\right) \tag{7a}$$

$$\frac{J}{n}(L, t|D, \Lambda^{1/2} v, \Lambda k, \Lambda k') = \Lambda^{1/2} \frac{J}{n}(\Lambda^{1/2} L, \Lambda t|D, v, k, k') \tag{7b}$$

so results for a range of arm lengths are required to access the effects of variations in D or k in terms of known effects of variations in v and k'.

UNIDIRECTIONAL TRANSPORT

Unidirectional transport occurs when the filament system is unipolar and all active particle motors have the same polarity. The mathematical description of this model is equivalent to theories of sedimentation or electrophoresis for a unimolecular reaction (Cann, 1970; Gilbert and Jenkins, 1959; van Holde, 1962). These theories often ignore free diffusion and focus on finding localized propagating solutions generated by nonlinear reaction kinetics. The binding of particles to filaments is a simple bimolecular reaction, for which the binding rate is a product of the concentrations of free particle and free binding sites and nonlinear in the above sense. For organelle transport, it can safely be assumed that particle concentrations are dilute, leading to Eqs. 1, which are linear in the concentrations. For these equations, stable traveling-wave solutions for a group of particles are not expected.

A unidirectional model follows from Eqs. 1 by setting $k_- = 0$, which is true when inward filaments are absent. The polarity subscript for rate constants for outward filaments is now omitted. Steady-state solutions are sought first, then transient solutions resulting from a step increase in particle concentration in the cell body, or a localized pulse injection of particles within a dendritic arm.

Steady-state solutions

Solutions of the steady-state form of the two remaining equations of (1), namely

$$-D\frac{\partial^2 n_o(x, t)}{\partial x^2} = -k n_o + k' n_+, \tag{8a}$$

$$v\frac{\partial n_+(x, t)}{\partial x} = k n_o - k' n_+ \tag{8b}$$

can be obtained by noticing that the flux $J = -D dn_o(x)/dx + n_+(x)v$ is independent of x (a first integral), giving the single differential equation

$$\frac{d^2 n_+(x)}{dx^2} + \frac{k'}{v}\frac{dn_+}{dx} - \frac{k}{D} n_+ = -\frac{Jk}{Dv} \tag{9}$$

for the bound concentration profile. The general solution can be written as

$$n_+(x) = \frac{J}{v} + Ae^{-q_+ x} + Be^{-q_-(x-L)} \tag{10a}$$

$$n_o(x) = \frac{J}{Kv} + \frac{A}{K}\left(1 - \frac{q_+ v}{k'}\right)e^{-q_+ x} + \frac{B}{K}\left(1 - \frac{q_- v}{k'}\right)e^{-q_-(x-L)} \tag{10b}$$

where

$$q_\pm = \frac{1}{2}\left\{\frac{k'}{v} \pm \sqrt{\left(\frac{k'}{v}\right)^2 + \frac{4k}{D}}\right\} \tag{11}$$

and $n_o(x)$ is obtained from Eq. 8b. The constants of integration A, B, and J follow by applying the first three boundary conditions of Eq. 5 for fixed free-particle concentrations n, $\tilde{n}$ at $x = 0$ and L, respectively (Fig. 1 *A*).

Irreversible attachment

When $k' = 0$, then $q_\pm = \pm q$, where $1/q = l_{off} = \sqrt{D/k}$ is the mean path length on filaments. Assuming that $L > l_{off}$, the boundary conditions yield $A = -kn/qv$, $B = k\tilde{n}/qv$, and

a net outward flux

$$J = n(v_D + \lambda v) \quad (v_D = \sqrt{kD}) \tag{12}$$

where v_D is a diffusional velocity, or diffusive displacement over the mean binding time $\tau_{off} = 1/k$. In contrast to transport by free diffusion, this flux is independent of the length of the arm. Because $\exp(-qL) \ll 1$, particles cannot diffuse freely down the whole arm without binding, and the flux is independent of particle concentration $\tilde{n}$ in the tip, even although such particles may diffuse back into the arm and bind to filaments. When the tip is closed and stationary, there is an accumulation of particles in the tip and steady-state conditions do not apply. If the tip is closed but extending at velocity u, then $J = \tilde{n}u$ and Eq. 12 determines the tip concentration $\tilde{n} = n(v_D + \lambda v)/u$, which will be higher than the cell-body concentration n if the arm is growing slowly.

Equation 12 expresses the outward steady-state flux in terms of the concentration n of free particles in the body, but this flux is conserved along the arm. Away from the cell-body end $x = 0$, all particles have bound to filaments and the flux is entirely due to motor transport. Thus the concentration of such particles is $n(v_D + \lambda v)/v$, since multiplication by v yields the predicted flux. This interior concentration is generally not equal to n; this can be understood as follows. With no loading in the cell body ($\lambda = 0$), the flux in the entrance to the arm where particles have not yet bound is entirely diffusional and proportional to the velocity v_D, which is usually slower than the motor speed v; as particles bind to filaments and are transported more rapidly at speed v, their lineal density is decreased if a steady state prevails. The disparity between the effective mobilities (flux per unit particle density) in the entrance and the interior of the arm is reduced when particles are loaded onto filaments in the cell body ($\lambda > 0$), but it should be remembered that the cell body then contains bound particles and the total density of such particles is $(1 + \lambda)n$. Such loading creates a parallel transport path in which particles remain bound throughout the entire outward journey, with a flux equal to $(\lambda n)v$.

The particle flux in the presence of motor filaments is generally much higher than from diffusion alone, $J_D = nD/L$ by Fick's law. The degree of facilitation

$$F \equiv \frac{J}{J_D} = (v_D + \lambda v)\frac{L}{D} \equiv \frac{L}{l_{off}}\left(1 + \lambda \frac{l_{pu}}{l_{off}}\right) \tag{13}$$

is much greater than unity even with no loading ($\lambda = 0$), except when the arm is shorter than l_{off}, which is under 1 μm for a 1-μm-diameter particle (Table 2).

Multiple attachments

With a finite detachment rate k', the expression for the flux is more complicated but differs little from Eq. 12 unless detachment is so rapid that the mean path lengths l_{off} and $l_{on} \equiv v/k'$ are similar. Assuming $|q_{\pm}L| > 1$, the complete expression for the net flux is

$$J = \left(1 - \frac{\lambda}{K}\right)\frac{2\xi}{1 + \sqrt{1 + (2\xi)^2}}nv_D + \lambda nv$$

$$\approx \left(1 - \frac{\lambda}{K}\right)nv_D + \lambda nv \quad (\xi \gg 1) \tag{14}$$

where $K = k/k'$ and $\xi \equiv Kv/v_D = l_{on}/l_{off}$ is the mean-path ratio, which is large if the motor speed is high or particles remain bound for long periods. The corresponding facilitation factor is

$$F = \frac{L}{l_{off}}\left\{1 + \frac{\lambda}{K}(\xi - 1)\right\} \quad (\xi \gg 1). \tag{15}$$

These results are very similar to Eqs. 12 and 13, which are recovered when $k' \to 0$. However, the formulae differ in detail. When $\lambda \ll K$, loading in the cell body is weak and particles must diffuse into the arm before binding; the flux is limited by the motor velocity v for slow motors ($v \ll v_D$) and by the diffusional velocity v_D in the opposite limit of fast motors. When $\lambda = K$, cell-body loading is optimal and the flux arises entirely from particles that bind before entering the arm (Fig. 2). These differences arise because, with reversible detachments, pathways into the arm by diffusion and cell-body loading are not independent.

Equations 10 show that the concentration profiles for free and bound particles within the arm are basically flat except at boundary layers of widths $1/q_+$ and $1/q_-$ at the ends. The absence of concentration gradients in the central zone shows that transport in this unidirectional model is clearly convec-

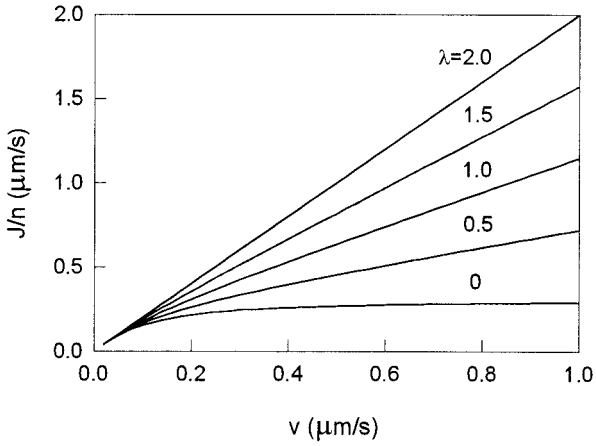

FIGURE 2 Unidirectional transport, steady state. The steady-state outward flux J in a cell arm per unit concentration n of free particles in the cell body as a function of motor velocity from Eq. 14, different loading parameters λ in the cell body as shown and $K = 2$. With no cell-body loading, the limiting flux of J/n at high motor speeds is the diffusional velocity $v_D = \sqrt{kD}$, here equal to 0.316 μm/s. With optimal loading ($\lambda = 2$), J/n is twice the motor velocity, reflecting the fact that the concentration of bound particles in the body is $2n$.

tive rather than diffusive, even though the flux is limited by diffusion into the arm when cell-body loading is ineffective. The concentrations of free and bound particles in the central zone are $n_o = J/Kv$, $n_+ = J/v$, showing that in this zone reaction-equilibrium is established with $n_+/n_o = K$, though not in the boundary layers. The flux J can therefore be interpreted in terms of the total concentration of particles $n_o + n_+$ in the central zone, moving at the mean speed

$$\bar{v} = \frac{K}{K+1} v \tag{16}$$

for particles with a duty ratio $K/(K + 1)$ (the bound steady-state fraction). Equation 15 shows that free diffusion in the free periods increases the central concentrations.

Transient solutions

The rise of flux in the tip

If the arm is initially free of particles, and particles are suddenly introduced at concentration n in the cell body ($x < 0$), there will be a time delay before particles arrive at the tip. If particles arriving in the tip region are prevented from diffusing back into the arm and rebinding, for example by imposing a cold block or sink, the tip response is measured by the net outward flux at the end of the arm. If the tip is closed and stationary, the response is measured by the concentration of particles in the tip. Although the latter may be closer to in vivo conditions, the tip concentration is sensitive to the value of $\tilde{\lambda}$, which is raised by mechanisms for storing particles in the tip region, so numerical calculations were made for the rise of flux in the presence of a sink at $x = L$. What behavior is expected?

In the unidirectional model, particles binding in the cell body will travel down an arm of length L in time L/v when no detachments occur ($L \ll l_{on} \equiv v/k'$). Initially free particles experience an extra delay of order of the binding time $1/k$, which will be partially offset if they can diffuse into the arm. In the opposite limit $L \gg l_{on}$, the rise time for flux at the tip should be approximately $L/\bar{v}$, where $\bar{v}$ is the mean displacement velocity (Eq. 16). These estimates ignore diffusion of free particles, which operate between pauses and should therefore speed up the rise of flux somewhat for short arms and weak binding ($K < 1$). Diffusion down the entire arm contributes negligibly to transport in long arms, since the rise time is of order $L^2/2D$, which is greater than $L/\bar{v}$ for $L > 2D/\bar{v}$, typically under 1 μm for microtubule motors with $\bar{v} \sim 1$ μm/s.

Fig. 3 shows the rise of flux at the end of a 20-μm arm, calculated for various rates of detachment that span the limiting cases described above. The time for the flux to rise to 50% of its final value is qualitatively described by the empirical formula $\tau_{0.5} \approx L/\bar{v}$. The computed rise time increases linearly with the length of the arm except for very short arms and rapid detachment, where the flux rise is more

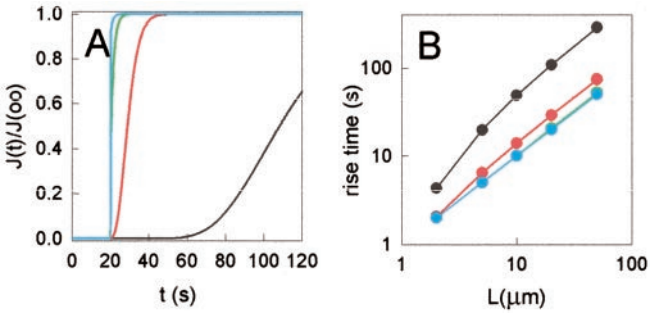

FIGURE 3 Unidirectional transport, stepwise increase of concentration in the cell body. (*A*) Rise of flux with time in the tip region of a 20-μm arm, initially without particles, after introducing unit concentration of particles in the body at time zero, for the unidirectional model for different rates of detachment $k' = 5$ (*black line*), 0.5 (*red line*), 0.05 (*green line*), and 0.005 s^{-1} (*blue line*). The motor speed is 1 μm/s, for which the full-transit time on filaments is 20 s, and $k = 1\ s^{-1}$, $D = 0.1\ \mu m^2/s$. Fluxes are normalized to their steady-state values calculated at long times, which agreed with the values predicted by Eq. 15. Numerical calculations were made by direct integration of Eqs. 1, using upwind differencing on the convective term (Press et al., 1992) and a smaller time step for the diffusion component. (*B*) Rise times to half the maximum flux as a function of arm length for the same set of detachment rates, plotted logarithmically (the *green* and *blue curves* overlap). Except at the highest rate of detachment and the second highest rate for the shortest arm, the results fit a linear law, as expected from the empirical formula given in the text.

rapid. This difference is due to free diffusion because it disappears when calculations are made with $D = 0$. There is also a spread of arrival times arising from pauses, which is most significant if $K < 1$, when particles are mostly paused. The length of each pause is controlled kinetically and obeys a Poisson distribution with a mean pause time of $1/k$. Conversely, when $K > 1$, a distribution of excursion times for bound particles is expected, but only if the arm is long enough to allow many attachment cycles; this condition was not fulfilled in calculations presented in the figure. Thus the computed rise times can be simply understood, but the dispersion of arrival times reflected in the shape of the flux-time curve requires a deeper analysis. Dispersive aspects of motor-assisted transport are considered next in relation to a different experimental protocol.

Dispersion from a point distribution

Distributions $p(x, t)$ of particle displacements x as a function of time t can be studied experimentally by tracking particles from their initial positions within the arm, or by injecting particles into the arm at one point. The form of these distributions may depend on whether the particles are initially free or bound, but the effects of initial conditions are removed after several cycles of attachment. For the unidirectional model, Fig. 4 shows the spatial distribution of particles for various motor speeds at a fixed time $t = 5$ s after injection of free particles at $x = 0$. The initial delta-function distribution is translated by motor action, and

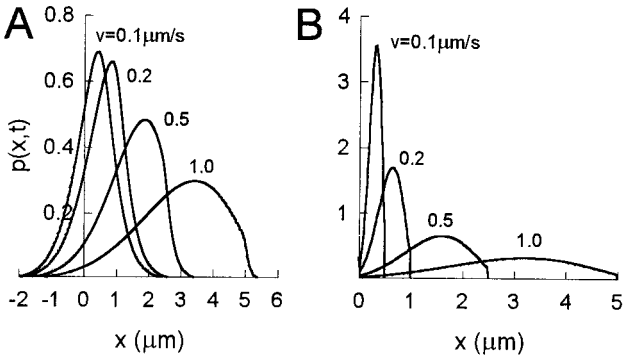

FIGURE 4 Unidirectional transport, dispersion. Computed distributions of particle displacement x in the middle of an infinite arm 5 s after starting at $x = 0$ with all particles detached from filaments. The two cases are (*A*) with free diffusion ($D = 0.1\ \mu m^2/s$), and (*B*) without free diffusion. The curves correspond to different motor speeds $v = 0.1$ to 1.0 μm/s as shown. The binding constant K was set at 2.0 and other parameters as in Table 2.

broadened by motor action and free diffusion before binding and during subsequent pauses. The figures show that single transits occur, producing a sharp right-hand edge in the distribution of displacements at $x = vt$ in Fig. 4 *B* when $D = 0$, although in Fig. 4 *A* this edge is broadened by free diffusion. The most probable displacement for each motor speed is close to the mean displacement $\bar{v}t$, where $\bar{v}/v = 2/3$ as $K = 2$.

The asymptotic form of these distributions at large times was not achieved in Fig. 4, but can be obtained analytically by Fourier-transform methods. The expected form after many attachment cycles is the classical diffusion law

$$p(x, t) \sim \frac{1}{\sqrt{4\pi D_* t}} \exp\left(-\frac{(x - \bar{v}t)^2}{4D_* t}\right) \tag{17}$$

about the asymptotic mean displacement $x(t) \sim \bar{v}t$, which also appears in theories of electrophoresis (Cann, 1970). The effective diffusion constant is

$$D_* = \frac{D}{K + 1} + \frac{K}{(K + 1)^2}\frac{v^2}{k + k'} \tag{18}$$

reflecting diffusion of free particles in solution and a Poisson distribution of bound periods. This result is also obtained from Eq. 4b by setting $K_- = 0$. The second term contains the variance of this Poisson distribution, proportional to $r(1 - r)$, where $r = K/(K + 1)$ is the bound fraction or duty ratio in attachment equilibrium. Diffusion is enhanced if $D_{on} > D$, where $D_{on} = v^2/(K + 1)(k + k') \equiv (v - \bar{v})^2/k'$, as expected from Eq. 4. When the duty ratio tends to unity at fixed k, D_{on} becomes small and particle motions approximate to uniform translation at the motor speed v.

The distribution (Eq. 17) was confirmed computationally by plotting a time-scaled distribution against a time-scaled displacement from the mean (Fig. 5), which asymptotes to the exponential factor in (17). At intermediate times, a truncated form of this distribution may appear because a significant fraction of displacements arise from full-transit events (those in which particles attach in the cell body and are transported to the tip without detachment) rather than multiple attachments, as can be seen in Fig. 5*B*, where free diffusion is absent.

Apart from this truncation effect, it turns out that the persistence of the effects of initial conditions, such as the proportion of particles initially bound, is felt only for the time $1/(k + k')$ required to bring free and bound particles into reaction equilibrium. No further change in the form of this distribution occurs over the cycling time $\tau_c = 1/k + 1/k'$, which is much larger than the equilibration time if $K \gg 1$. Thus the initial equilibration of free and bound particles is all that matters, and subsequent attachment cycles merely produce dispersion about the average velocity $\bar{v}$ according to Eq. 17. This feature is peculiar to the unidirectional model; very different behavior is found with bidirectional models.

The persistence of initial conditions is also reflected in the time-dependence of low-order moments

$$\overline{x(t)^n} = \int_{-\infty}^{\infty} x^n p(x, t)dx \tag{19}$$

of the distribution, in particular the mean displacement $\overline{x(t)}$ and variance $S(t) = \overline{x(t)^2} - \overline{x(t)}^2$. For the models of this paper, these functions can be calculated exactly, from the appropriate differential equations (Appendix A) or by Fou-

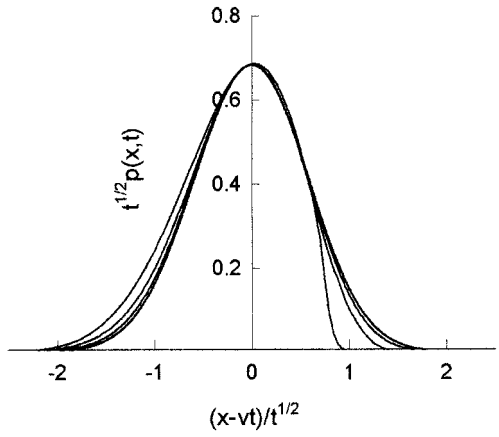

FIGURE 5 Unidirectional transport, dispersion at long times. The approach to a Gaussian distribution of scaled deviations $y = (x - \bar{v}t)/t^{1/2}$ from the mean displacement for particles spreading from a point distribution, as in Fig. 4 with $v = 1$ μm/s. The indicated distribution slowly approaches the function $(4\pi D_{eff})^{-1/2} \exp(-y^2/4D_{eff})$ from Eq. 17 (results shown are for $t = 5$, 20, 100, and 1000 s). The standard deviation of the last curve (0.341 μm) is close to the value $2D_{eff} = 0.363$ from Eq. 18 with $D = 0.1\ \mu m^2/s$, $k = 1\ s^{-1}$, $k' = 0.5\ s^{-1}$. The first curve shows the truncation effect seen in Fig. 4 and associated with single excursions.

rier methods. The former method is more efficient. For the unidirectional model,

$$\overline{x(t)} = \bar{v}t + \left(p - \frac{K}{K+1}\right)\frac{v}{k+k'}(1 - e^{-(k+k')t}) \quad (20a)$$

$$S(t) = 2D_* t + A(1 - e^{-(k+k')t}) + B(1 - e^{-2(k+k')t}) + Cte^{-(k+k')t} \quad (20b)$$

where p is the initial fraction of bound particles and D_* is given by Eq. 18. The constants A, B, C are given in Eqs. A6. There is an initial temporal phase reflecting the bound fraction that persists for the equilibration time, followed by a second phase of diffusion about the mean, which lasts indefinitely (Fig. 6). Endogenous particles are expected to be in kinetic equilibrium with their filaments ($p = K/(K+1)$), in which case there is no transient in the mean displacement and the variance-time curve approaches linearity with a single exponential function ($B = C = 0$); the predicted behavior for injected particles ($p = 0$) is more complex. These predictions could be tested by fitting experimental moment-time curves obtained from an ensemble of tracked-particle distributions; the same method has been used for bead assays of kinesin motility (Svoboda et al., 1994).

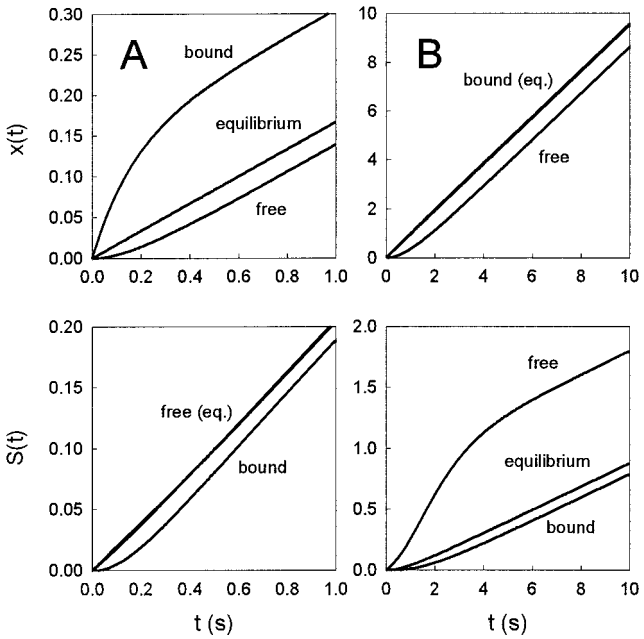

FIGURE 6 Unidirectional transport, time-dependence of the mean displacement $\overline{x(t)}$, and variance $S(t)$ in the unidirectional model, calculated from Eqs. 20 with $k' = 5\ s^{-1}$ (A) and $0.05\ s^{-1}$ (B), and values of D, v, and k in Table 2. The initial transients are functions of the initial particle state, either free ($p = 0$), bound ($p = 1$), or an equilibrium mixture ($p = K/(K+1)$). Memory of the initial state persists over a time of order $1/(k + k') = 0.17$ s (A) or 0.95 s (B).

SYMMETRIC BIDIRECTIONAL TRANSPORT

The reaction-diffusion-transport equations (1) define a general bidirectional transport model. Here we consider only the symmetric case, taking $k_+ = k_- \equiv k$, $k'_+ = k'_- \equiv k'$ and $v_+ = -v_- \equiv v$. This symmetric model describes particles with only one type of motor moving on a bipolar filament network with an equal mixture of polarities, for example myosin-V on F-actin. The same model could also be used for a unipolar filament network if particles possess two kinds of motors with opposite polarity but the same motor speed, and the same attachment and detachment rates, which may be approximated by kinesin and dynein motors on microtubules. The relevance of these models is further considered in the Discussion section, but we attempt to address both systems by presenting computation results for a range of motor speeds and detachment rates. The binding rate and diffusion constant are usually fixed in the following examples at $1\ s^{-1}$ and $0.1\ \mu m^2/s$, but the scaling laws (Eqs. 7 and 8) are structured in such a way that predictions for lower values of both these quantities can also be obtained.

As before, steady-state transport properties are investigated first, followed by transient responses and dispersive behavior.

Steady-state solutions

Irreversible attachment

Bound particles are likely to proceed down the arm in a single pass when $L \ll l_{on}$, which is possible with microtubule motors in short arms (under 10 μm). Here we consider the limiting case $k' = 0$. The steady-state solutions of the symmetrized form of Eqs. 1 are

$$n_o(x) = ne^{-qx} + \tilde{n}e^{q(x-L)},$$

$$n_+(x) = \lambda n + \frac{kn}{qv}(1 - e^{-qx}) + \frac{k\tilde{n}}{qv}e^{q(x-L)}$$

$$n_-(x) = \tilde{\lambda}\tilde{n} + \frac{kn}{qv}e^{-qx} + \frac{k\tilde{n}}{qv}(1 - e^{q(x-L)}) \quad (21)$$

where $1/q = l_{off} = \sqrt{D/2k}$ and $qL \gg 1$. From Eq. 2, the net outward flux is

$$J = n\left(\frac{v_D}{2} + \lambda v\right) - \tilde{n}\left(\frac{v_D}{2} + \tilde{\lambda}v\right). \quad (22)$$

The diffusion velocity $v_D \equiv l_{off}/\tau_{off}$ is now equal to $\sqrt{2kD}$, but only half of the particles entering the arm bind to filaments directed into the arm as required; the remainder are returned by motor action to their starting points.

With a sink at the tip ($\tilde{n} = 0$), Eq. 22 has the same structure as Eq. 13 for unidirectional transport and the discussion underneath applies in equal measure. When the tip concentration $\tilde{n}$ is not held fixed and the arm is closed,

the "no-flux" condition at the outer end is achieved when the concentration of free particles has risen to its steady-state value

$$\tilde{n} = \frac{v_D + 2\lambda v}{v_D + 2\tilde{\lambda} v} n \tag{23}$$

for which $J = 0$. Under these conditions, particles are exchanged by motor action on both filaments, at a rate J_{ex} obtained from bound-state fluxes in the central zone of the arm away from boundary layers, as

$$J_{ex} = n\left(\frac{v_D}{2} + \lambda v\right) = \tilde{n}\left(\frac{v_D}{2} + \tilde{\lambda}\tilde{v}\right). \tag{24}$$

This rate of exchange equals the net rate of outward transport with a sink at the tip. The way in which transport is shared between free diffusion and motor action in the loading zones is shown in Fig. 7 for both types of boundary conditions at the tip.

Multiple attachments

When $L > l_{on}$, particles detach and rebind many times before traversing the arm. Steady-state solutions of Eqs. 1 can be obtained from the equivalent equations

$$D\frac{d^2 n_o(x)}{dx^2} = 2kn_o - k'n_1, \tag{25a}$$

$$v\frac{dn_1(x)}{dx} = -k'm, \tag{25b}$$

$$v\frac{dm(x)}{dx} = 2kn_o - k'm \tag{25c}$$

where $n_1(x) = n_+(x) + n_-(x)$, $m(x) = n_+(x) - n_-(x)$. From Eq. 2, $J = -Ddn_o/dx + vm(x)$ is x-independent, so $n_o(x)$ can be eliminated from Eq. 25c, giving a single second-order equation

$$\frac{d^2 m(x)}{dx^2} - Q^2 m(x) = -\frac{2kJ}{vD}, \quad \left(Q^2 = \frac{2k}{D} + \left(\frac{k'}{v}\right)^2\right). \tag{26}$$

Note that $Q = 1/l$, where $l^{-2} = l_{off}^{-2} + l_{on}^{-2}$ and l is a mean path length for establishing kinetic equilibrium. Solutions satisfying the boundary conditions (Eqs. 4) also simplify when $QL > 1$, which is implied by the defining inequality of this subsection. In terms of the ratios

$$\varepsilon = k'/Qv \equiv l/l_{on}, \qquad \eta = v/k'L \equiv l_{on}/L \tag{27}$$

where $\varepsilon, \eta < 1$, the concentration profiles are obtained from

$$m(x) = Ae^{-Qx} + Be^{Q(x-L)} - (1 - \varepsilon^2)\frac{J}{v} \tag{28a}$$

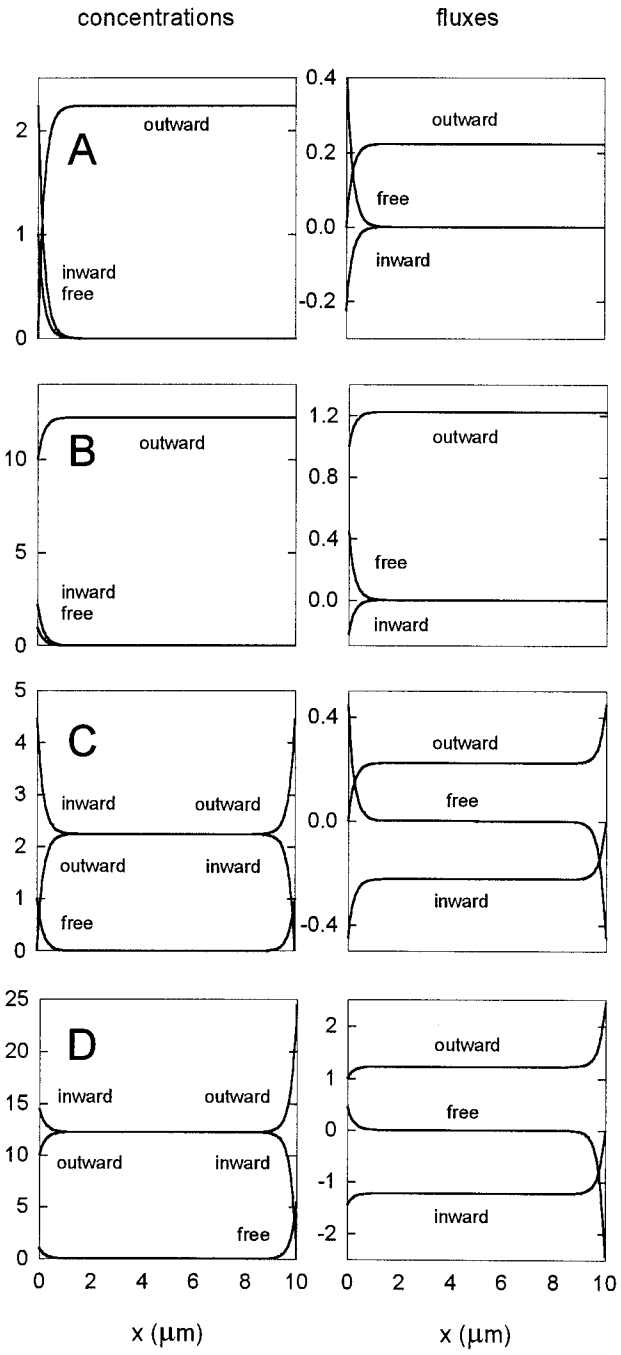

FIGURE 7 Bidirectional transport, steady state. Concentration profiles and the corresponding fluxes of free particles and bound particles on outward/inward filaments with irreversible attachment to filaments, from Eqs. 2a and 11, shown for the case of a sink at the tip ($\tilde{n} = 0$, rows *A* and *B*) and with the tip closed ($J = 0$, rows *C* and *D*). In *A* and *C* the loading efficiency λ is zero, implying that the filaments of the arm do not extend back into the cell body ($l_{pu} = 0$), and $\lambda = 10$ in *B* and *D*. Particle parameters are as in Table 2 with $v = 0.1$ μm/s, so $l_{pu} = 2$ μm when $\lambda = 10$. The body concentration n was set to unity, and the loading parameter $\tilde{\lambda}$ in the tip to zero. With a sink at the tip, the net outward flux is 0.224 particles/μm^2 · s in *A* and 1.224 in *B*, giving facilitation factors of 22.4 and 122.4 above free diffusion over the same distance of 10 μm. With a closed tip, the capture ratio $\tilde{n}/n$ for particles in the tip was 1.0 in case *C* and 5.48 in case *D*, as determined from Eq. 23.

$$n_1(x) = n_1(0) - (1 - \varepsilon^2)\frac{Jx}{\eta v L} + A\varepsilon(1 - e^{-Qx}) + B\varepsilon e^{Q(x-L)}, \quad (28b)$$

$$n_o(x) = \frac{v}{2k}\frac{dm(x)}{dx} + \frac{n_1(x)}{2K}. \quad (28c)$$

which, with boundary conditions (Eqs. 4), yield the net flux

$$J = \frac{n - \tilde{n} + (1 - \varepsilon^{-1})K^{-1}(\lambda n - \tilde{\lambda}\tilde{n})}{1 + 2(1 - \varepsilon)\eta}\frac{D}{\varepsilon L} \quad (29)$$

and the integration constants A, B, $n_1(0)$ given under Fig. 8. Equation 2 gives the corresponding fluxes from the concentration profiles. The net flux J is inversely proportional to arm length L, just as for pure diffusion. Terms of order $\exp(-QL)$ have been dropped, but those of order $\eta = l_{on}/L$ must be retained because J reflects the difference $m(x)$ in particle populations on outward and inward filaments, which must satisfy the correct boundary conditions. For sink conditions ($\tilde{n} = 0$), the flux facilitation factor can be written as

$$F \approx \left(1 - \frac{\lambda}{K}\right)\frac{l_{on}}{l} + \frac{\lambda}{K}\left(\frac{l_{on}}{l}\right)^2 \quad (30)$$

neglecting terms of order η. Thus $F > 1$ when $l_{on} > l$, where the equilibration length l is below l_{off}. If particles can load on outward filaments starting within the cell body, F is increased again to a maximum value $(l_{on}/l_{off})^2$ when the loading factor λ has its maximum value K, achieved when $l_{pu} \gg l_{on}$ (Eq. 6).

Fig. 8 shows examples of concentration profiles and fluxes in the arm. There is a central zone in which free and bound particles are in reaction equilibrium with $n_1(x)/n_o(x) = 2K$, with boundary layers of width l_{off} at each end. Multiple attachment cycles produce quasi-diffusive transport characterized by a linear fall in free and bound concentrations down the arm, while a single irreversible attachment produces convective transport characterized by a flat concentration of bound particles (Fig. 7). The solution described above can be clearly seen in a central zone where all concentrations fall linearly with x. Hence particle transport in this zone can be described by Fick's law in the form

$$J = -D_*\frac{dn(x)}{dx} \quad (31)$$

where $n(x) = (2K + 1)n_o(x)$ is the total particle concentration at position x, and

$$D_* = \frac{D}{2K + 1} + \frac{2K}{2K + 1}\frac{v^2}{k'}, \quad (32)$$

the symmetric version of Eq. 4 *B*, is the compound diffusion constant. Again, diffusion is enhanced when $D_{on} > D$, where $D_{on} = v^2/k'$. In contrast to the unidirectional case, this diffusion constant becomes very large as K is increased at fixed k (the duty ratio tends to unity). As K is increased from zero at fixed k, D_* initially decreases to a minimum where the high detachment rate forces $D_{on} < D$, but then increases without bound as D_{on} becomes very large (Table 2). This behavior is in contrast to the unidirectional model, where D_{on} tends to zero in the high duty ratio limit.

The flux is still limited by the boundary layer near $x = 0$, which determines how the free concentration profile $n_o(x)$ matches onto the cell-body concentration. When the degree of loading is small, particles must diffuse into the arm to bind to filaments, thus establishing a boundary layer with a significant drop in free-particle concentration across it. Conversely, the boundary layer almost disappears when particles are efficiently loaded in the cell body ($\lambda \approx K$). This is confirmed by assuming that the boundary layer is absent, so $dn_o(x)/dx = n/L$ with a sink at the tip and $J = (2K + 1)D_*n/L$. The resulting facilitation factor $1 + (l_{on}/l_{off})^2 \equiv (l_{on}/l)^2$ is just as predicted by Eq. 30.

With a closed tip, the net outward flux in the arm is zero under steady-state conditions, but particles are still exchanged between the cell body and the tip. The path of a particle in the arm is complicated by binding to filaments of random polarity, but a rate of exchange on filaments may be defined as before, giving

$$J_{ex} = n\left\{\left(1 - \frac{\lambda}{K}\right)\sqrt{1 - \varepsilon^2}\frac{v_D}{2} + \lambda v\right\} \quad (33)$$

which is different from Eq. 24 in much the same way that Eqs. 12 and 14 for unidirectional transport differ from each other.

Table 3 summarizes our predictions for rates of outward transport and the corresponding facilitation factor for both unidirectional and bidirectional transport models with a sink at the tip. The linear nature of the basic transport equations (1) ensures that predictions with a fixed positive concentration in the tip can be obtained by superimposing the inverted solution in which cell body and tip are interchanged. Hence Fick's law, in the form that the net outward flux is proportional to the concentration difference $n - \tilde{n}$, applies only to the completely symmetric model for bidirectional transport, namely the model presented in this section but with equal loading factors at each end.

Transient solutions

The rise of flux in the tip

When particles make a complete transit along the arm without detaching, the rise times of flux at the outer end in the presence of a sink are of order L/v for unidirectional and bidirectional models. For bidirectional systems, the sink prevents particles from reloading onto inward filaments. However, when multiple detachments occur, the direction of motor action can be reversed at random, as determined by

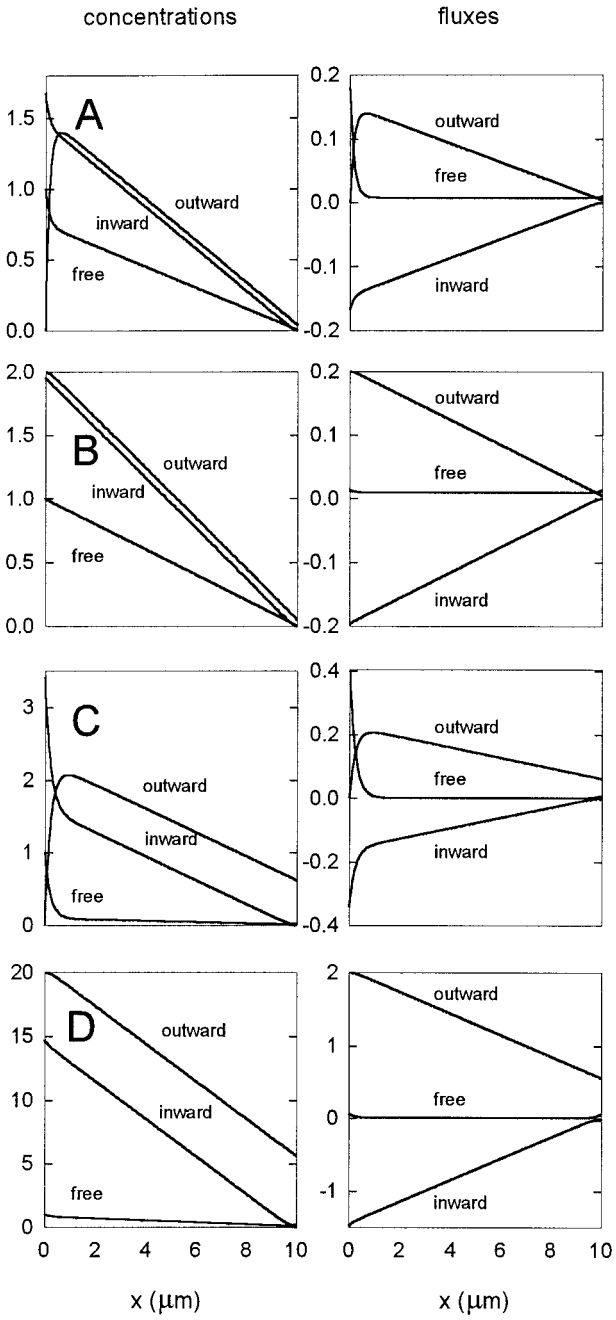

FIGURE 8 Bidirectional transport, steady state. Concentration profiles and fluxes along the cellular arm of length 10 μm when particles detach frequently within the arm, allowing multiple excursions on filaments of either polarity. The tip concentration is held at zero, and the rate constant k' for detachment is 0.5 s^{-1} in *A* and *B* and 0.05 s^{-1} in *C* and *D*. Other fixed parameters are as in Fig. 7. The loading parameter λ is zero in *A* and *C*, otherwise set to its maximum value $K = k/k'$, giving $\lambda = 2.0$ ($l_{pu} = 1.52$ μm) in *B* and $\lambda = 20$ ($l_{pu} = 20$ μm) in *D*. The flux facilitation factors are 1.33, 1.78, 6.64, and 59.8 for cases *A–D*, respectively. All concentrations fall linearly with position over most of the arm, since the mean path length l_{on} (0.2 μm in *A* and *B*, 2 μm in *C* and *D*) is less than the length of the arm. All profiles were calculated from Eqs. 2, 28, and 29, where the coefficients in Eq. 28 satisfy $A = -2\varepsilon(K - \lambda)n/(1 + \varepsilon) - \varepsilon(1 - \varepsilon)J/v$, $A + B = -2\varepsilon K(n - \tilde{n})/(1 - \varepsilon^2) + \varepsilon J/\eta v$, and $n_1(0) = 2(\varepsilon K + \lambda)n/(1 + \varepsilon) - \varepsilon(1 - \varepsilon)J/v$. Terms containing the flux J may be small, of order l_{on}/L, but must be retained to satisfy the boundary conditions (Eq. 5).

random choices of filament polarity or motor type at the instant of binding. These shuttling motions may be considered as random walks. In the limit of many pauses the distribution of the net displacement can be obtained from the central limit theorem, even though the length of each excursion on filaments is itself a random variable controlled by the kinetics of detachment (Chandrasekhar, 1943). If the length of each excursion is approximated by the mean path length $l_{on} = v/k'$, the most probable displacement after N steps is of the order of $N^{1/2}l_{on}$ in either direction, so $N \sim (L/l_{on})^2$. Thus the rise time is estimated by $N\tau_c$ where $\tau_c = 1/2k + 1/k'$, or

$$\tau_{0.5} \approx \left(\frac{Lk'}{v}\right)^2\left(\frac{1}{k'} + \frac{1}{2k}\right) \quad (L \gg l_{on}) \tag{34}$$

neglecting diffusion in the pauses.

Computer solutions of the symmetric case of Eqs. 1 for a step rise in particle concentration in the cell body give flux-time curves (Fig. 9) similar to those found for the unidirectional model (Fig. 3), but with certain characteristic differences. In agreement with Eq. 34, calculated rise times vary quadratically rather than linearly with arm length in most cases, the exceptions being for lower rates of detachment and/or short arms, where it can be seen that multiple attachments are not expected. For the same detachment rate, this effect is more pronounced at the higher motor velocity (1.0 against 0.1 μm/s) where the mean excursion length is longer. In most cases the rise time is a decreasing function of the detachment rate, but at the lower motor velocity the rise time increases when k' is changed from 5 to 0.5 s^{-1} (*black* to *red lines* in Fig. 9 *A*) and this effect persists over the range of arm lengths used with a quadratic variation of rise time with length. This effect appears to arise from free diffusion in the pauses, which operate to maximum effect in shortening the rise time when the duty ratio is below unity and the motor speed is low, and is not present in parallel calculations made with $D = 0$. This conclusion is also supported by Eq. 7a, which predicts that the flux-time curve with a 100-fold reduction in D has the same shape as that with the original diffusion constant, and a 10-fold increase in motor velocity and arm length (set $\Lambda = 0.1$ and replace v with v/Λ).

Dispersion from a point distribution

The symmetric bidirectional model produces, as would be expected, a symmetric distribution of particle displacements moving away from an initial point distribution (Fig. 10). These distributions generally show more structure than for unidirectional transport, and are shown to evolve through three distinct phases with characteristic profiles. If the particles are initially free, they may disperse by diffusion in the cytoplasm before binding, followed by an intermediate phase after the first binding event, where particles can motor

TABLE 3 Summary of formulae

	$\lambda = 0$		$\lambda = K$	
	J/n	F	J/n	F
Free diffusion	D/L	1	D/L	1
Unidirectional $k' \ll v/L$	$\sqrt{kD}$	L/l_{off}	$\sqrt{kD} + Kv$	$(L/l_{off})(1 + (l_{on}/l_{off}))$
Unidirectional $k' > v/L$	$\dfrac{2Kv}{1 + \sqrt{1 + \dfrac{4Kv^2}{Dk'}}}$	$\dfrac{L/l_{off}}{\sqrt{1 + \left(\dfrac{l_{off}}{2l_{on}}\right)^2} + \dfrac{l_{off}}{2l_{on}}}$	Kv	Ll_{on}/l_{off}^2
Bidirectional $k' \ll v/L$	$\sqrt{kD/2}$	$L/2l_{off}$	$\sqrt{kD/2} + Kv$	$(L/2l_{off})(1 + (l_{on}/l_{off}))$
Bidirectional $k' > v/L$	$(D/L)\sqrt{1 + (2Kv^2/Dk')}$	l_{on}/l	$(D/L)(1 + (2Kv^2/Dk'))$	$(l_{on}/l)^2$

Formulae for the steady-state flux J down an arm of length L with end concentrations n and zero, and the corresponding facilitation factors $F = JL/nD$ over free diffusion, for minimum and maximum loading onto filaments at the central end ($\lambda = 0$ and K, respectively). Predictions for intermediate values of λ are correctly given by linear interpolation. The mean path lengths are $l_{on} = v/k'$, $l^{-2} = l_{off}^{-2} + l_{on}^{-2}$, where $l_{off} = (D/k)^{1/2}$ for the unidirectional model and $(D/2k)^{1/2}$ for the bidirectional model. Other symbols are defined in Table 1. Note that filament density and its effect on the value of K may need to be taken into account in direct comparison of the uni and bidirectional cases.

in either direction out of the diffusive peak if $\xi > 1$. In contrast to unidirectional transport, the following cycles of attachment produce excursions of random direction and random magnitude, producing a third and final phase that asymptotes to a classical diffusion law when the number of cycles becomes large. Following the discussion of the unidirectional model, one can expect that the intermediate phase sets in after the equilibration time $1/(2k + k')$ and the final "compound-diffusion" phase after times in excess of the cycle time $\tau_c = 1/2k + 1/k'$. The gap between these characteristic time scales defines the persistence of the intermediate phase, which can be very prolonged if $k' \ll k$. With these estimates, the distributions shown in Fig. 10 lie between the second and third phases, but the time elapsed is clearly insufficient to establish the Gaussian distribution that describes compound-diffusion behavior because the shape of the distribution depends on motor speed.

A full discussion of this behavior requires specific initial and final particle states $i, j = 0, \pm$ (free or bound to either filament). The corresponding distributions are the Green's

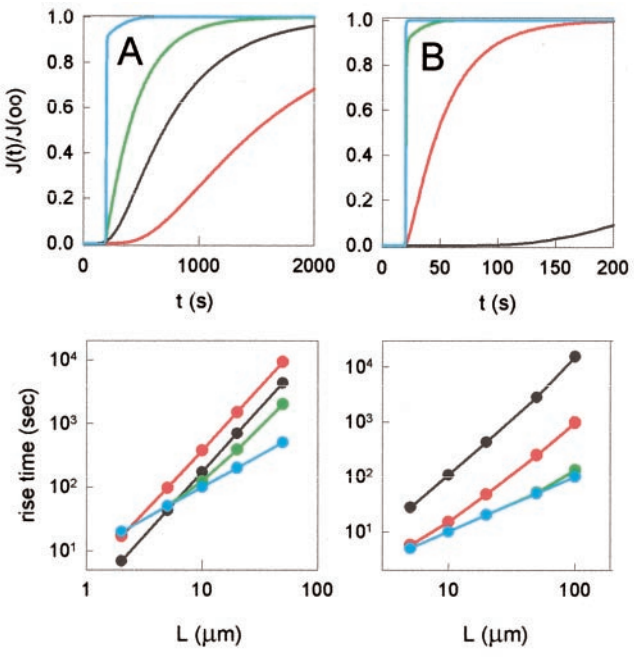

FIGURE 9 Bidirectional transport, stepwise increase of concentration in the cell body. The rise of flux at the tip of a 20 μm arm (*upper boxes*) and the corresponding rise times over a range of arm lengths (*lower boxes*), computed for motor speeds of 0.1 (*A*) and 1.0 μm/s (*B*). The curves correspond to different detachment rates, as in Fig. 3. The corresponding rise times are seen to vary quadratically with arm length whenever many attachment cycles occur within the arm, as discussed in the main text.

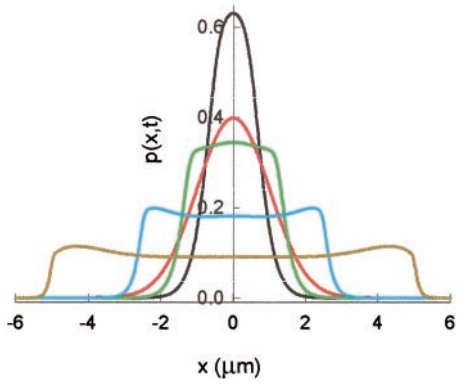

FIGURE 10 Bidirectional transport, dispersion. Computed distributions of particle displacement x in the middle of an infinite arm, 5 s after starting with all particles at $x = 0$ and detached from filaments, showing the effects of different motor speeds $v = 0$ (*black line*), 0.1 (*red line*), 0.25 (*green line*), 0.5 (*blue line*), and 1.0 μm/s (*khaki line*). Other parameter values are as given in Fig. 4. At the highest motor speed, the distribution shows shallow twin peaks close to the single-excursion displacements (± 5 μm).

functions or propagators $G_{ij}(x, t)$ of the problem, and

$$p(x, t) = \sum_{i,j} G_{ij}(x, t)p_j \tag{35}$$

where p_j is the probability of the initial state j. For $t > 0$ they satisfy the same reaction-diffusion-convection equations (1) as the concentrations (McQuarrie, 1962). For the initial phase, the displacement distributions are given by the functions

$$g_o(x, t) = \frac{1}{\sqrt{4\pi Dt}} \exp\left(-\frac{x^2}{4Dt} - 2kt\right),$$
$$g_{\pm}(x, t) = \delta(x \mp vt)\exp(-k't). \tag{36}$$

where $i = j$ so only one state label is required. The probabilities $\exp(-2kt)$, $\exp(-k't)$ of surviving binding or detachment respectively define the lifetimes of the initial states. For distributions after the initial binding or detachment event, numerical calculations are required. We used three separate computational approaches, namely full numerical solution of Eqs. 1 using smaller time steps for free diffusion than for kinetics and upwind differencing (Press et al., 1992) for motor action, a Fourier transform method with numerical inversion of the time transform, and a partial perturbation expansion for the intermediate phase in powers of the rate constants k, k', reducing to simple closed formulae when $D = 0$ (Appendix B).

Fig. 11 shows a representative set of distribution functions calculated for $D = 0.1\ \mu m^2/s$, $v = 0.1\ \mu m/s$, $k = 1\ s^{-1}$, various detachment rates, and particles either free or equally bound to filaments of both polarity. The initial bound-state distribution is equal to $(g_+ + g_-)/2$, which comprises propagating functions of zero width not shown in the figure. All other contributions are continuous functions in which the particle has changed its attachment state at least once.

When $K < 1$, the bound fraction or duty ratio $r = 2K/(2K + 1)$ is small and the distribution appears to maintain its diffusion-like character at all times (Fig. 11 *A*). A distinct intermediate phase showing the presence of a "motoring" population appears for $K > 1$, first as a plateau with discontinuous borders (Fig. 11 *B*) and then as sharply peaked but continuous distributions near $|x| = vt$ for $K \gg 1$ (Fig. 11 *C*). The change in shape from a plateau to distinct peaks as K increases reflects the shift from free to bound particles during the major part of the time interval. When $K > 1$, the forms of these distributions depend on the initial state (free or bound) and define the intermediate phase of motor-assisted diffusion, which lasts for approximately one cycle of binding/detachment. The average cycle time $\tau_c = 1/2k + 1/k'$ becomes large as k' is decreased ($K \gg 1$). In this limit, the heights of the peaks decrease with time if the particle is initially free, representing the first detachment event. If the particle is initially bound, then one cycle of binding and detachment is necessary to reach the intermediate phase as defined above, and the probability of one kinetic cycle grows in time over the interval $(0, \tau_c)$. Increasing the motor speed and hence ξ produces similar effects to the same increase in K (results not shown).

The transition from the intermediate phase to compound diffusion can also be studied analytically by expanding the propagators in powers of the number of attachment cycles (Appendix B). Thus the rounded plateau distribution found with $K = 2$ and particles initially bound (Fig. 11 *B*) is characteristic of particles starting on a track of one polarity and finishing on a track of opposite polarity; the probability of doing this rather than remaining on the same track is high if the duty ratio is not too large. The distribution for this process actually turns out to be symmetric in x even when the starting track has given polarity; this results from equal divisions of the time interval $(0, t)$ spent on plus- and minus-directed tracks. Appendix B also shows that the lifetime of the intermediate phase also depends on the initial state.

After many attachment cycles, any initial bias in the net direction of transport is removed and the displacement distribution tends to the classical diffusion law

$$p(x, t) = \frac{1}{\sqrt{4\pi D_* t}} \exp\left(-\frac{x^2}{4D_* t}\right) \tag{37}$$

where D_* is the compound diffusion constant in Eq. 32. The final phase is not apparent in Fig. 11 except perhaps at very low duty ratio (case *A*), where the intermediate phase is absent and compound diffusion is not markedly different from the initial phase of free diffusion. To demonstrate the existence of compound diffusion, distribution functions were again computed out to many cycle times and the function $t^{1/2}p(x, t)$ plotted against $y = x^2/t$ for various times. After many cycles, these functions converge to a universal Gaussian function independent of the initial state (Fig. 12).

There is no characteristic onset time (in the sense of an exponential process) for compound diffusion. A particle initially on an outward filament will typically move by about one mean free path l_{on} over time τ_{on}. The additional time Δt required for this displacement to be obliterated by compound diffusion is that the standard deviation exceed the initial displacement, or

$$D_*\Delta t \gg l_{on}^2. \tag{38}$$

This condition can be rewritten as $\Delta t \gg (1 - \varepsilon)^2\tau_c$, where τ_c is the mean cycle time and $\varepsilon = l/l_{on}$. For $\varepsilon \ll 1$, many cycles of detachment and rebinding are required.

As before, moments of the distribution provide some information about the underlying processes. For symmetric bidirectional transport, the first moment is identically zero, while the second moment or variance is given by

$$S(t) = 2D_*t + A(1 - e^{-k't}) + B(1 - e^{-(2k+k')t}) \tag{39}$$

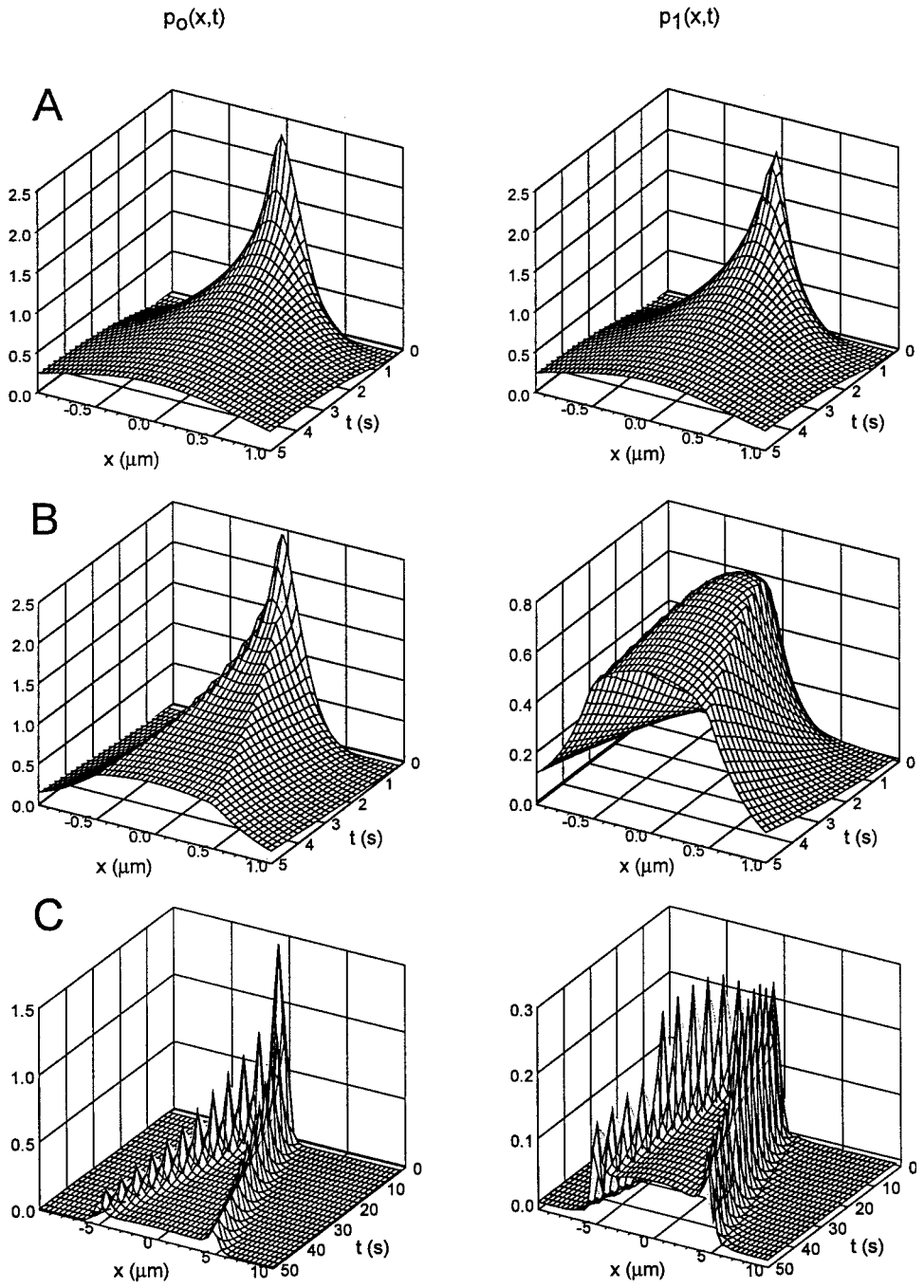

FIGURE 11 Bidirectional transport, dispersion. The computed space-time behavior of particle displacement distributions $p_i(x, t)$ in an arm, starting at $x = 0$ and either detached ($i = 0$) or equally bound to filaments of each polarity ($i = 1$), showing the effect of different detachment rates $k' = 5$ (*A*), 0.5 (*B*), and 0.05 s^{-1} (*C*). The motor velocity is set at 0.1 μm/s, with other parameters as in Table 2.

The long-time behavior obeys the expected diffusion law with the compound diffusion constant of Eq. 32, and the coefficients *A*, *B* depend on the initial state (Eqs. A8). This result differs from Eq. 20b for unidirectional transport; there is a slower exponential process at the detachment rate k', which terminates the intermediate phase. If observed displacement distributions of tracked particles can be fitted to Eq. 39 by adjusting the five parameters involved, the initial bound fraction and the four basic parameters D, v, k, k' of the symmetric bidirectional model could be obtained.

Fig. 13 shows that the variance first rises linearly as $2Dt$ if particles are initially detached, or quadratically as $(vt)^2$ from motor action of initially bound particles, the initial slope being zero. For particles initially in equilibrium, there is only one exponential decay and insufficient information to determine the four basic parameters; thus injection of free particles or tracking of initially bound particles is required. For highly processive motors ($k' \ll k$), the two exponentials are well separated in time and long-lived motor action appears as an extended quasi-quadratic curve before detach-

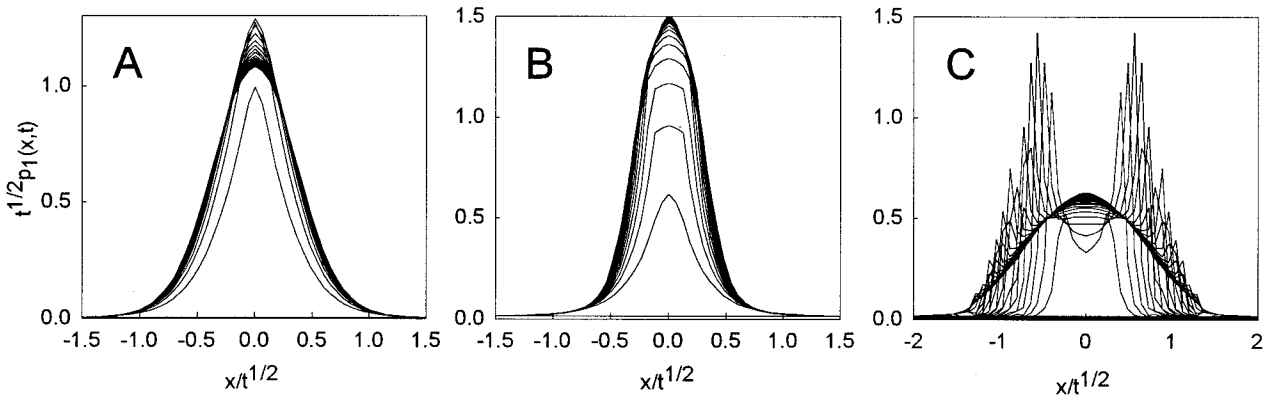

FIGURE 12 Bidirectional transport, dispersion. The approach to compounded diffusive behavior. Plots of the scaled distributions $t^{1/2}p_1(x, t)$ against $y = t^{-1/2}x$ for 25 equally spaced time intervals out to time t_{max} = 5, 20, and 200 s in *A–C* for k' = 5, 0.5, and 0.05 s^{-1}, respectively, and other parameters as in Fig. 11. After many attachment cycles, the curves coalesce to the universal Gaussian curve $(4\pi D_*)^{-1/2} \exp(-y^2/4D_*)$ with values of D_* in Table 2 as determined by Eq. 32. The average number of cycles t_{max}/τ_c is equal to 7.1, 8.0, and 9.8 for cases *A–C*, respectively.

ment produces the asymptotic linear behavior for $t \gg 1/k'$. In this case, binding of initially free particles also produces a knee in the curve much earlier on, at times $\sim 1/2k$. The linear law applies at times greater than the cycle time and permits the compound diffusion constant to be determined. Thus the variance-time curve displays the three predicted phases, which should be useful indicators of motor kinetics.

COMPARISONS WITH EXPERIMENT

It may be useful to start by summarizing the main predictions of the unidirectional and symmetric bidirectional models. For numerical illustrations, consider a microtubule-like example with $L = 50$ μm, $v = 0.5$ μm/s, $k' = 0.05$ s^{-1}, $K = 20$, using $D = 0.1$ $\mu m^2/s$ as discussed in Table 2. At this juncture, we revert to the terminology of cell biology: the cell body and a tip are proximal and distal ends, respectively, of a cell axon or dendritic arm; outward and inward transport are respectively anterograde and retrograde.

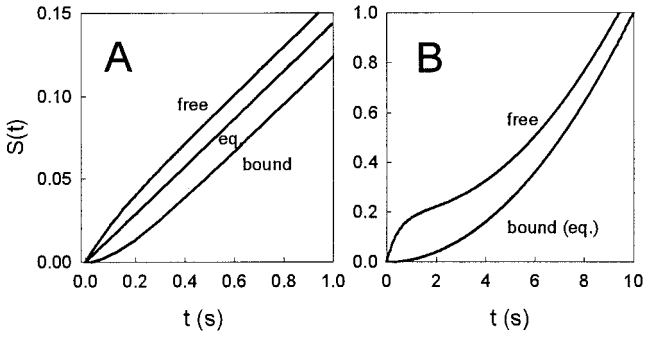

FIGURE 13 Bidirectional transport, dispersion. Time-dependence of the displacement variance $S(t)$, calculated from Eqs. 39 and A8, for motor-assisted diffusion in the limits of low and high duty ratios ($K = 0.2$ in *A* and 2000 in *B*) and values of D, v, and k in Table 1. The initial transients are functions of the initial state, either free ($p = 0$), bound equally to filaments of both polarities ($p = 1$), or an equilibrium mixture of the first two cases ($p = 2K/(2K + 1)$). The linear law $S(t) = 2D_*t$ is achieved asymptotically after many attachment cycles. In *B*, the cycling time is very large and the quadratic law seen for initially bound vesicles reflects the intermediate phase, where bound particles stay on one filament.

First, in the unidirectional model with an anterograde filament-motor system, the flux of particles in an arm is driven by the particle concentration in the cell body, independent of the tip concentration. The steady-state flux per particle is equal to the motor velocity if the duty ratio is high and particles are efficiently loaded onto filaments in the cell body. If the duty ratio or the motor velocity is low, the flux is increased if the particles can diffuse freely in the pauses. In the symmetric bidirectional model, the net anterograde flux is a decreasing function of particle concentration in a distal region; however, this region must be accessible to the ends of filaments in the arm and the flux is enhanced if an auxiliary filament system is present. In that case, a net flux proportional to the concentration difference between the ends (Fick's law) applies only if the loading factors at each end of the arm are equal. With equal loadings and end concentrations there is no net flux, but particles are exchanged between the ends at a rate that can approach the motor velocity.

Second, with a distal sink, the relative transport capacities of the two models can be gauged from Table 3. As might be expected, anterograde fluxes for the two systems are very similar for short arms, where most particles can be transported in a single excursion; then $J^{(bi)}/J^{(uni)} \leq 1$, the precise value depending on pre-loading. For longer arms allowing multiple attachments, the unidirectional system is faster because the bidirectional flux is inversely proportional to the length of the arm. For example, for microtubule-like filaments where $l_{on} \gg l_{off}$, $J^{(bi)}/J^{(uni)} \approx l_{on}/L < 1$, namely 0.2 in the above example. As a general rule, optimal pre-loading of particles in the cell body can increase the flux by

the ratio l_{on}/l_{off} of the free path lengths, equal to 45 for the "microtubule" parameters.

Third, if there is a step increase of particle concentration in the cell body, the concentration at the end of an arm of length L equilibrates in a time of order $L/\bar{v}$ (103 s) for the unidirectional model when the duty ratio r is near unity, and $L^2/2D_*$ (510 s) for the bidirectional model where the diffusion constant D_* (4.9 $\mu m^2/s$ in the present example) includes the effects of many motor displacements of random sign. A smaller step increase may occur at time L/v, where v is the motor velocity. Since $\bar{v} = rv$, the main peak will be much delayed if the duty ratio is low, but in that case the equilibration time in short arms may be smaller if unbound particles can diffuse freely. A comparison of these formulae for the unidirectional and bidirectional cases in arms of the same length suggests that the latter equilibrates more slowly when $L > 2D_*\bar{v}$, or 4.7 μm in the above example. However, this estimate is correct only if $L > l_{on}$, here equal to 10 μm, so the first estimate must be revised upward.

Fourth, in the bidirectional model, tracked particles disperse from their initial positions with a variance that grows quadratically in time over the first period of motor action if the duty ratio is high, moving to a linear law only after many attachment cycles. The diffusion of free particles produces a linear law at all times, apparent if the duty ratio is low. In contrast, the unidirectional model also gives a net flux of tracked particles, moving initially at the motor velocity v but falling to the average velocity after kinetic equilibrium is established. If the duty ratio is high, this equilibration time is much less than the mean lifetime of particles bound to filaments. Distributions of displacements make corresponding changes in form with elapsed time, reaching a diffusion law about the mean position only after many cycles of attachment.

Although flux rates are generally inferior with bidirectional transport, it has to be borne in mind that there may be a wider functional significance of bidirectionality, for example in retaining particles or achieving a uniform distribution. In some cases this may be a consequence of an effective diffusion constant D_* that is lower in value than the free diffusion constant for the particle, namely when $v^2/k' < D$, which is possible for slow motors and/or a low duty ratio.

Comparisons with experimental data should be made in light of a number of factors reflecting the complex nature of the interactions between particles, filaments, and the cytoplasmic environment generally. To this end, we briefly review existing motility data for axons, melanocytes, and melanophores, keeping in mind the present models. When a single one-dimensional filament system is dominant, there is usually no difficulty in fitting either the unidirectional model or a symmetric bidirectional model to displacement-time data in the sense of assigning values of the four basic parameters v, k, k', and D. However, the data reveal two possible inadequacies with the models; the apparent diffusion constant of organelles detached from motor-filaments is much smaller than expected from free diffusion, and the speed of organelles motoring on filaments appears to fluctuate within each period of motor action. These problems are evaluated in the concluding discussion: in general terms, they are connected with the origins of pauses between periods of motor action.

Axonal transport

In nerve axons, bidirectional transport of various intracellular organelles, including vesicles, mitochondria, and the endoplasmic reticulum, occurs on microtubules that may be up to 100 μm in length (see Breuer et al., 1988). The microtubule system is unipolar, or almost completely so, with "plus" ends directed outward (Baas and Yu, 1998; Heidemann et al., 1981, 1984), and bidirectional transport is produced by plus-end and minus-end motors (kinesin and dynein, respectively) on each organelle. It is important to establish whether only one kind of motor on each organelle is activated at the same time. If kinesin is switched on by a regulatory agent in the cell body and dynein switched on in the nerve terminals, then organelles in the axon showing anterograde and retrograde motions can be considered separately, using the unidirectional model in which every pause is followed by motion in the same direction. Conversely, both kinds of motor could be simultaneously active but bound to different parts of the organelle, leading to coherent motor action in a direction chosen at random by its current orientation, which is seen to change for nonspherical organelles (Koles et al., 1982; see also Hayden et al., 1983). If pauses produced by detachment and rebinding generate fairly frequent reversals, the bidirectional model would be indicated. In axonal transport, there are reports of pauses occasionally followed by intermittent reversals, but never over distances above a few microns (Cooper and Smith, 1974), on the whole supporting the unidirectional model. However, the coupling effects of motion on actin filaments also need to be considered.

Displacement-time plots $x(t)$, typically collected at time intervals $\delta t = 0.2$–1 s, are commonly analyzed to give the distribution of coarse-grained velocities $\delta x/\delta t$. For endogenous particles, these distributions typically show a broad range of velocities heavily biased in one direction, a narrower peak centered about zero, and a peak at zero velocity, representing particles bound and motoring on filaments, particles diffusing freely or attached to moving structures, and particles trapped on static structures, which could also be motor-filaments (Adams and Bray, 1983; Allen et al., 1982; Bridgman, 1999; Breuer et al., 1988; Cooper and Smith, 1974; Koles et al., 1982; Morris and Hollenbeck, 1995). Similar distributions have been observed for injected proteins (Buchner et al., 1987; Galbraith et al., 1999 and references therein). The mean velocity $\bar{v}_B$ during bound periods can provisionally be interpreted as a lower estimate

for the motor speed v of the particle. The two may not be equal because, even if the particle travels at constant speed v on a motor-filament, short periods of detachment and rebinding may be hidden by the finite sampling time. The maximum velocity or leading edge of the distribution is an upper bound to the motor velocity, but may arise from rare events such as elastic recoil of filaments (Allen et al., 1982), so may not be a reliable estimate of v. Some authors also give the mean path length l_{on} traveled over bound periods or the maximum path length observed, which may be much greater (a Poisson distribution is expected). Then lower and upper bounds for the mean detachment rate $k' = v/l_{on}$ can be obtained, which validate such measurements of motor velocity if $k'\delta t \ll 1$, taking $k < k'$.

Data for anterograde transport and particle diameters of 0.2–0.7 μm from the above sources give mean bound speeds $\bar{v}_B = 0.30$–2.5 μm/s and $v_{max} = 1$–5 μm/s. To some extent, these variations correlate with particle size. For particles above and below 0.5 μm diameter, respectively, Breuer et al. (1988) find $\bar{v}_B = 0.3$ and 0.7 μm/s, $v_{max} = 1.0$ and 2.7 μm/s, $l_{on} = 2.11$ and 3.14 μm, and duty ratios $r =$ 0.24 and 0.21. These values are sufficient to bracket the motor velocities, the detachment rates k' between (0.15–0.5) and (0.2–0.8) s^{-1}, respectively, and binding rates k between (0.05–0.15) and (0.06–0.23) s^{-1} using $r = k/(k + k')$. In this investigation the sampling time δt was 0.11–0.25 s, so that $k'\delta t \ll 1$ and detachment and rebinding during one sampling period is rare and can be ignored. Thus fluctuations in motor speed in each interval between pauses appear to be present.

The effects of the actin network on axonal transport are now well known: the motor involved is myosin V (Tabb et al., 1998). This network supports long-range axonal transport in the absence of microtubules, but although all particles on the same actin track move in the same direction, over all filaments this mechanism is inherently bidirectional. Estimated motor velocities again vary widely, from 0.07 to 3.0 μm/s. Values above 0.4 μm/s (the motor velocity for myosin Va from in vitro motility assays) are observed in extruded axoplasm (Allen et al., 1982; Kuznetsov et al., 1992, 1994), where the filament network may not be stationary. Reported mean excursion lengths range from 0.5 to 4 μm (Kuznetsov et al., 1992; Bruer et al., 1988; see also Rodionov et al., 1998) and are generally shorter than on microtubules (3–10 μm). In the absence of obstructions, the detachment rate should be faster than from microtubules, suggesting that organelles reaching the actin network undergo many cycles of detachment and rebinding to actin before they are re-captured by a microtubule. Over one cycle of microtubule motor action, the detached organelle may be considered to be in kinetic equilibrium with actin, so that free organelles and organelles undergoing motor-assisted diffusion on F-actin may be lumped together. Then the unidirectional model with microtubules is valid if the free diffusion constant D is replaced by $(1 - p_A)D + p_A v_A^2/k'_A$, where p_A is the equilibrium probability of the organelle-actin complex and v_A and k'_A are the organelle's motor speed and detachment rate on actin. The binding rate k to microtubules would also be reduced by a factor p_A with respect to the axon in which actin has been removed.

Coupling effects between the two filament systems have been studied by Morris and Hollenbeck (1995), using normal axons and axons in which microtubules or actin filaments had been depolymerized. With no microtubules, reversals of the motions of particles on the actin network were observed. Motor velocities estimated from bound periods sampled every second were similar in both directions, namely 0.3–0.4 μm/s in normal axons, 0.2 μm/s on actin alone, and 0.6 μm/s on microtubules only. That the motor velocity in the dual-filament system is smaller than that on microtubules alone suggests either that not all particles analyzed were on microtubules, or that the mean excursion length on microtubules was shortened by contacts with actin filaments. Mean excursion lengths were not given, while the maximum values reported in each direction are not correlated with removal of microtubules. For all three systems the motor speeds in each direction are nearly equal, suggesting that the net direction of transport is sensitive to differences in the corresponding duty ratios, giving net anterograde transport in wild-type axons and retrograde transport in the actin-only system, although the microtubule-only system is almost symmetric with respect to motor velocity and duty ratio.

Melanocytic dendrites

Axial transport of melanosomes in the dendritic arms of melanocytes is now recognized as another bidirectional dual transport system, containing microtubules near the central axis and subcortical actin filaments (Wu et al., 1998). Bidirectional long-range transport is observed in the presence of myosin V and also in its absence (as in the "dilute" mouse mutation, Wei et al., 1997), indicating that at least one microtubule motor must be present. Whether this bidirectionality arises from plus- and minus-end motors or from microtubules of opposite polarity is still an open question; microtubule bundles in axonal dendrites are equipolar (Baas and Yu, 1998) so we tentatively assume that this is the case in melanodendrites. Bidirectional transport also occurs on the actin network alone. Apparent motor velocities for the dual system, the dilute mutation (motor action on microtubules only), and the actin-only system, namely 0.7, 1.0–1.1, and 0.14 μm/s, respectively, are again similar in both directions. Mean path lengths on microtubules were 12–13 μm; those on actin were not reported, but appear to be above 0.3 μm. Thus, in most respects this dual transport system appear similar to that in axons. There are similar reservations about the low value of the velocity on actin.

The accumulation of a high concentration of melanosomes in dendritic tips is required physiologically for trans-

fer to keratinocytes in the epidermis, which occurs only when the actin-(myosin V) system is active (Wu et al., 1998). In the "dilute" mutation, most melanosomes remain in the central cell body; some travel back and forth in dendrites but almost none are captured in the tip (Provance et al., 1996; Wei et al., 1997). These observations can be understood in terms of filament geometries in the cell body and the tip, which serve to load melanosomes on to the fast transport system in the arm (microtubules). A high concentration of particles in the tip relative to the central cell body can be achieved if loading is efficient in the cell body but inefficient in the tip, as exemplified in the bidirectional model with $\lambda > \tilde{\lambda}$ from Eq. 23 for short arms or a similar equation derived from Eq. 33 for long arms. In the central cytoplasm, Wu et al. have found that melanosomes load onto short microtubules (average length ~ 3 μm) feeding those in the arm, which is the mechanism considered in Fig. 1. In the tips of dendrites, a somewhat different argument is required.

In the absence of a cortical actin network under the tip, it is reasonable to expect that a particle arriving at the end of an anterograde microtubule would detach and bind to a retrograde microtubule rather than diffuse into the tip space. In this case loading is efficient, but the effective capture volume in the tip is much smaller than its actual volume, however defined, being limited by the diffusion length of melanosomes in the close vicinity of retrograde microtubules. Whatever the concentration of melanosomes in this capture volume, the concentration averaged over the whole tip volume would be very small. The presence of actin filaments in the tip, mainly localized under the membrane but with projections toward microtubule termini, should therefore act to capture a much higher number of particles in the tip volume, as suggested by Wu et al. For the tip volume, the situation is as envisaged in Fig. 1 with no projecting microtubules, and hence inefficient loading ($\tilde{\lambda} = 0$). The purpose of the submembrane actin system in the tip is to spread, and thereby store, melanosomes throughout the tip region. It would be useful to model this system directly.

If dendrites contain an equipolar mixture of microtubules, then bidirectional transport could be produced by microtubule motors of only one polarity on melanosomes, and the symmetric bidirectional model would presumably apply to transport on each filament system, giving motor-assisted diffusion. This could be tested by an analog of the classical diffusion experiment, in which the net anterograde particle flux is proportional to the difference in concentrations between the central body and the tip region.

Melanophores

Particle tracking experiments on higher-dimensional actin networks have been carried out in melanophores, notably by Rodionov et al. (1998) who measured the distribution of net displacements in any direction after 30 s. Their observations can be qualitatively described by the radial distribution function for two-dimensional diffusion

$$p(r, t) = \frac{\Gamma(d) r^{d-1}}{(4\pi D_* t)^{d/2}} \exp\left(-\frac{r^2}{4D_* t}\right) \tag{40}$$

(Carslaw and Jaeger, 1959) for $d = 2$, although the tail of the observed distribution is broader. Setting the most probable distance $\sqrt{2(d-1)D_* t}$ after time t to 0.5 μm with $t =$ 30 s yields $D_* = 0.0042$ μm^2/s. Can this value be understood in terms of motor-assisted diffusion on a randomly polarized two-dimensional filament system?

Equation 40 is valid only if many attachment cycles occur over the observation period. The authors observe tortuous particle tracks, suggesting $l_{on} < 0.5$ μm as required and $v =$ 0.07 μm/s, giving $k' = v/l_{on} > 0.14$ s^{-1} and more than four attachment cycles over 30 s. The generalization of Eqs. 1 to arbitrary dimensions predicts that

$$D_* = (1 - r)D + r\frac{v^2}{k'd} \quad \left(r = \frac{\Gamma K}{1 + \Gamma K}\right), \tag{41}$$

where r is the duty ratio and $\Gamma(d) = 2, 2\pi, 4\pi$ for $d = 1, 2,$ 3. The observed diffusion constant can be accounted for if $k' = 0.59$ s^{-1} and $k \gg k'$ ($r \sim 1$). It would be interesting to know if the spread of displacements is bigger at longer times, or whether there is a time-independent component of the distribution which reflects the presence of short actin filaments.

The apparent diffusion constant is so small that it could also arise from hindered diffusion of free particles in the cytoplasm, were it not for the near absence of such motions when the actin system was removed. If the first explanation is basically correct, the observed diffusion constant must be compatible with Eq. 40 for duty ratios just below unity, which mix in a small proportion of free-diffusion behavior. When viewed in this way, the observed value of D_* constrains the free diffusion constant D to similar values or less, about two orders or magnitude smaller than expected from Stokes' law (Table 2). Presumably, many free particles are intermittently trapped by static components of the cytoskeleton.

Melanophores are also a dual filament system, with biased bidirectional transport on a microtubule network projecting radially from the cell nucleus (Rogers et al., 1997). Centrifugal transport on this system acts to move pigment bodies from the center to the semi-cortical actin system, where they are dispersed to approximate a uniform distribution of dark matter (Rodionov et al., 1998; Rogers and Gelfand, 1998). The conditions for achieving a uniform steady-state distribution should reflect the spatial distribution of filament density in the cell, and two-dimensional models could be investigated.

CONCLUDING DISCUSSION

The previous section shows that many features of organelle transport in axons, melanocytes, and melanophores are compatible with the reaction-diffusion-transport models presented, in which particle convection occurs on a filament system and is due to the action of molecular motors. This mechanism, rather than mechanisms based on cytoplasmic streaming, is also indicated by the identification of organelle motors specific to the dual filament systems observed in many types of cell motility (Langford, 1995; Kelleher and Titus, 1998). For some applications, the models should clearly be generalized to include a dual filament system and/or actin networks of higher dimensionality. There are many aspects of organelle movements not described by the basic models (Weiss et al., 1986), which raises the question of what features should be added without destroying their simplicity, and hence their utility. Two particular deficiencies suggest specific improvements: 1) there is evidence that the motor speed of the organelle fluctuates while remaining bound to a filament, and 2) diffusion of organelles not bound to motor filaments is absent or is much slower than expected from the Einstein-Stokes formula. It is necessary to show that these features are compatible with the kind of organelle movements expected from motor action when attached to a filament, and from the laws of diffusion when they are not. If this can be done, then the way is open for the development of better models, perhaps allied to more detailed observations.

Regarding 1) above, fluctuations in the speed of an organelle apparently remaining bound to a motor filament could be due to many undetected short pauses or fluctuations in the number of motor molecules in strong interaction with the filament. The second explanation seems more probable, as it does not require all motors to detach simultaneously. In motility assays where a filament moves on a field of tethered motor molecules, the steady velocity is observed to decrease as the surface density of motors is reduced (Winkelmann et al., 1995). Steady motion may also be replaced by fluctuating motion if the motors are insecurely tethered, particularly at low densities. Assays where a single motor molecule moves an attached bead (Svoboda et al., 1993) suggest that kinetic fluctuations in the number of motors bound to a filament should be less severe for highly processive motors such as kinesin or myosin V, where a single dimeric motor may stay within a zone of weak interaction around the microtubule for many cycles of ATP hydrolysis (Hackney, 1995; de la Cruz et al., 1999). It seems unlikely that all motors on a many-motor organelle will be simultaneously detached unless the organelle is physically removed from the interaction zone by Brownian forces or otherwise. Organelle translocation speeds would fluctuate if the organelle changes orientation or moves momentarily away from the filament, thereby changing the number of motors in instantaneous interaction with the filament. This hypothesis could be tested from high-resolution images that track one particle on an unencumbered filament.

Koles et al. (1982) have suggested that velocity fluctuations arise from spatial variations in cytoplasmic viscosity. However, motor speeds on an isolated filament are expected to be load-independent for micron-sized particles and normal cytoplasm; the tension/velocity coefficient for viscous drag is two orders of magnitude smaller than the slope of the load-velocity line, namely 5 pN · s/μm for kinesin (Svoboda and Block, 1994).

Regarding 2) above, organelles diffusing in the cytoplasm are observed to remain stationary for long periods, perhaps because they become trapped on secondary cytoskeletal structures such as intermediate filaments. Clearly, free diffusion at rates compatible with formulae based on the Einstein-Stokes relation can occur when the particle is clear of size-excluding compartments (Provance et al., 1993) and trapping structures. The model could be extended to include trapped states, but the kinetics of transitions between free and trapped states would need to be dictated by the system studied. Organelles may also be blocked if the filament on which they move is entangled.

Before returning to macroscopic models, it would be useful to have a reasonably comprehensive model for the trajectory of a single organelle. Such a model would necessarily be stochastic, but would need to describe more random events than the models of this paper, which require a stochastic interpretation of attachment events when applied to a single particle. A general aim of this kind of model would be to relate the observed trajectory to the architecture of the cytoskeleton, so that the state of motion at each instant can be correlated with local cytoskeletal structures. Automatic methods for analyzing trajectories in this way are desirable to identify trapped or blocked periods and any intrinsic fluctuations in motor speed within periods of unblocked motor action. For example, spatial fluctuations in a two-dimensional trajectory could be analyzed for components parallel and perpendicular to a smoothed trajectory, to distinguish motoring states from freely diffusing states. If fluctuations in motor speed are seen to be intrinsic to the interaction between organelle and motor filament, the interaction could be modeled as a stochastic process, possibly specified by the velocity autocorrelation function. Such a model would predict the distribution of displacements, or at least their mean and variance, as a function of time for an ensemble of trajectories, or individual trajectories on a Monte Carlo basis.

Finally, classical macroscopic models that generalize those presented in this paper can be reconstructed from models of a single trajectory, perhaps as above, that detect the positions of trapping and blocking structures in the process of analyzing the observed motion. These models require a second level of averaging over details of spatial structures such as the actin network and trapping or exclud-

ing objects. For size-excluding compartments, transport throughout the whole intracellular volume is still described by Fick's law, but with a reduced diffusion constant; various models exist which relate this constant to compartment structure (Dayel et al., 1999; Hou et al., 1990; Janson et al., 1996; Olveczky and Verkman, 1998). However, this description lumps free and trapped states together, and there may be cases in which it is better to recognize a trapped state explicitly, with a kinetic description of transitions between the two states. If blocked states also exist, then a comprehensive classical theory of organelle motion, with all spatial averaging in place, would require four kinds of organelle states (1 = free, 2 = motoring, 3 = trapped, 4 = blocked), with non-zero rate constants for transitions $1 \leftrightarrow 2$, $1 \leftrightarrow 3$, and $2 \leftrightarrow 4$, and a stochastic description of fluctuating speeds in the motor state. As stated, the free and trapped states might be combined by renormalizing the diffusion constant downward. The blocked state might also be lumped with the motoring state by renormalizing the mean motor velocity downward, but this procedure is somewhat dangerous unless the correct interpretation is kept clearly in mind.

APPENDIX A

The equation-of-motion method for displacement moments

Differential equations of motion for the displacement moments (Eq. 19) can be derived from the reaction-diffusion-transport equations. These equations are closed because the rate constants are independent of particle position. The method is general, and in this context gives an efficient way of calculating low-order moments.

Let $M_{ni}(t)$ be the nth displacement moment of the joint distribution $p_i(x, t)$ which also predicts the probability of particle state i at time t. Its time derivative is obtained by taking the nth moment with respect to x of Eqs. 1, and integrations-by-parts to remove the space derivatives in diffusion and convection terms. Hence

$$\frac{dM_{no}(t)}{dt} = n(n-1)DM_{n-2,o} - (k_+ + k_-)M_{no} + k'_+M_{n+} + k'_-M_{n-} \quad \text{(A1a)}$$

$$\frac{dM_{n\pm}(t)}{dt} = nv_\pm M_{n-1,\pm} + k_\pm M_{no} - k'_\pm M_{n\pm} \quad \text{(A1b)}$$

are valid for $n = 0, 1, 2, \ldots$ if $M_{no} \equiv 0$ for $n < 0$. Then

$$\overline{x(t)^n} = M_{no}(t) + M_{n+}(t) + M_{n-}(t) \quad \text{(A2)}$$

including $n = 0$, where the moments are state probabilities which sum to unity and obey purely kinetic equations. The initial values at $t = 0$ are zero except for $n = 0$, and $p = M_{n+}(0) + M_{n-}(0)$ is the initial bound fraction. Hence

$$\frac{d\overline{x(t)}}{dt} = v_+M_{o+} + v_-M_{o-} \quad \text{(A3a)}$$

$$\frac{d\overline{x(t)^2}}{dt} = 2(DM_{oo} + v_+M_{1+} + v_-M_{1-}) \quad \text{(A3b)}$$

When the first moment is non-zero, it is convenient to work directly with the equation of motion for the variance $S(t)$, namely

$$\frac{dS(t)}{dt} = 2DM_{oo} + 2\sum_\pm v_\pm(M_{1\pm} - \overline{x(t)}M_{o\pm}) \quad \text{(A4)}$$

which shows which moments are required. Solutions for the two specialized forms of the model are summarized below.

Unidirectional model

Here $k_+ = k$ and $v_+ = v$, $k_- = 0$, so $M_{n-} \equiv 0$, giving $M_{oo}(t) = (1-p)e^{-st} + (1-r)(1-e^{-st})$, $M_{o+}(t) = pe^{-st} + r(1-e^{-st})$, where $r = K/(K+1)$ and $s = k + k'$, giving Eq. 20a of the main text for the mean displacement. An equation of motion for M_{1+} can then be found by using Eq. A2 to eliminate M_{1o}, giving

$$M_{1+}(t) = rvt + (p-2r)(v/r)(1-e^{-st}) + (1-r)(p-r)vte^{-st} \quad \text{(A5)}$$

Integration of Eq. A4 gives the variance function in Eq. 20b with coefficients

$$A = (r-p)\frac{2D}{s} + \frac{2v^2}{s^2}\{p(1-p) - 2r(1-r)\},$$
$$B = (p-r)^2\frac{v^2}{s^2},$$
$$C = -(1-2r)(p-r)\frac{2v^2}{s}. \quad \text{(A6)}$$

Symmetric bidirectional model

With $k_\pm = k$, $k'_\pm = k'$, and $v_\pm = \pm v$, these symmetries force $2M_{o\pm}(t) = M_{o1}(t)$, which behaves as does $M_{o+}(t)$ in the unidirectional case, but with $r = 2K/(2K+1)$. For the same reasons, $\overline{x(t)} = M_{1o}(t) = M_{11}(t) = 0$. Hence $dM_{1\pm}(t)/dt = \pm vM_{o\pm} - k'M_{1\pm}$, for which

$$M_{1\pm}(t) = \pm\frac{v}{2}\left\{\frac{r}{k'}(1-e^{-k't}) - \frac{(p-r)}{2k}(e^{-st} - e^{-k't})\right\} \quad \text{(A7)}$$

where $s = 2k + k'$. These moments are an odd function of filament/motor polarity. The second moment or variance satisfies $dS(t)/dt = 2DM_{oo} + 4vM_{1+}$, leading to Eq. 39 of the main text with coefficients

$$A = -\left(\frac{2r}{k'} + \frac{r-p}{k}\right)\frac{v^2}{k'}, \quad B = \frac{r-p}{s}\left(2D + \frac{v^2}{k}\right) \quad \text{(A8)}$$

The second term is zero when the particles are initially in equilibrium ($p = r$).

APPENDIX B

An expansion in powers of the number of cycles

The Green's functions of the infinite one-dimensional case satisfy integral equations that generate an expansion in powers of the number of kinetic cycles over time t. This solution defines the intermediate phase in the time

evolution of the distributions, particularly in the limit $D \to 0$, where simple closed formulae can be obtained. The technique is described below for the symmetric bidirectional model.

The integral equations

$$G_{oo}(x, t) = g_o(x, t) + k' \sum_{\sigma=\pm} \int_0^t dt' \int dx' \, g_o(x - x', t - t') G_{\sigma o}(x', t'), \quad \text{(B1a)}$$

$$G_{\sigma o}(x, t) = k \int_0^t dt' \int dx' \, g_\sigma(x - x', t - t') G_{oo}(x', t'), \quad \text{(B1b)}$$

$$G_{o\mu}(x, t) = k' \sum_{\sigma=\pm} \int_0^t dt' \int dx' \, g_o(x - x', t - t') G_{\sigma\mu}(x', t'), \quad \text{(B1c)}$$

$$G_{\sigma\mu}(x, t) = g_\sigma(x, t)\delta_{\sigma\mu} + k' \int_0^t dt' \int dx' \, g_\sigma(x - x', t - t') G_{o\mu}(x', t') \quad \text{(B1d)}$$

where (σ, $\mu = \pm$) are the solutions of the symmetric version of Eqs. 1 for $t > 0$. The functions $g_i(x, t)$ in Eq. 36 can be used to construct an iterative solution of which the leading terms are

$$G_{oo}(x, t) - g_o(x, t) = kk' \sum_{\sigma=\pm} \int_0^t dt' \int_0^{t'} dt'' \iint dx' dx'' \, g_o(x - x', t - t') g_\sigma(x' - x'', t' - t'') g_o(x'', t'') + O(kk')^2, \quad \text{(B2a)}$$

$$G_{\sigma o}(x, t) = k \int_0^t dt' \int dx' g_\sigma(x - x', t - t') \, g_o(x', t') + O(k^2 k'), \quad \text{(B2b)}$$

$$G_{o\mu}(x, t) = k' \int_0^t dt' \int dx' g_o(x - x', t - t') \, g_\mu(x', t') + O(kk'^2), \quad \text{(B3c)}$$

$$G_{\sigma\mu}(x, t) - g_\sigma(x, t)\delta_{\sigma\mu} = kk' \int_0^t dt' \int_0^{t'} dt'' \iint dx' dx'' \, g_\sigma(x - x', t - t') g_o(x' - x'', t' - t'') g_\mu(x'', t'') + O(kk')^2. \quad \text{(B2d)}$$

Each term in the right-hand side is derived from its predecessor by an extra cycle of attachment that introduces an extra power of kk'. For G_{oo}, the first such term describes free diffusion from 0 to t'', binding with probability kdt'' to either track, motor transport on that track from t'' to t', detachment with probability $k'dt'$ and free diffusion from t' to t, summed over intermediate times and positions. The next term (not shown) involves two cycles of binding and detachment. For the off-diagonal propagators, the leading term requires a single binding or detachment event between times 0 and t.

This expansion is not simply a Taylor series in kk' because the lifetimes of the states are built into the "unperturbed" propagators g_o, $g_\pm$; successive terms describe only transitions into the final state, but transitions out of the final state are already included. The leading terms can be identified with the intermediate phase of vesicle propagation, which must be preceded either by one cycle of attachment if the initial and final states are equal, otherwise by one binding/detachment event. These considerations determine the onset time of the intermediate phase in terms of the rate constants k, k'. The same rate constants also determine the lifetime of this phase, so it is appropriate to build them into the unperturbed propagators. Higher-order terms in the expansion can be neglected when the duty ratio is large and cycling is slow ($k' \ll k$ and $\tau_{on} \gg \tau_{off}$). However, higher-order terms must become important at long times, where repeated cycling produces compound diffusion; thus the above expansion is expected to converge only for the intermediate phase.

In the limit of large vesicles, $D \to 0$ and $g_o(x, t) \to \delta(x)\exp(-2kt)$, so all propagators in the intermediate phase defined above can be calculated exactly from Eq. B2. Including initial terms, we find that

$$G_{oo}(x, t) \approx e^{-2kt}\left\{\delta(x) + \frac{2kk'}{v}\left(t - \frac{|x|}{v}\right)e^{(2k-k')|x|/v}\vartheta(vt - |x|)\right\},$$

$$G_{+o}(x, t) \approx \frac{k}{v} e^{(2k-k')|x|/v - 2kt}\vartheta(vt - |x|),$$

$$G_{-+}(x, t) \approx \frac{kk'}{2(2k - k')v} e^{-k't}(1 - e^{(2k-k')(|x|/v - t)})\vartheta(vt - |x|),$$

$$G_{++}(x, t) \approx \delta(x)e^{-k't} + \frac{kk'x}{v^2} e^{(2k-k')|x|/v - 2kt}\vartheta(vt - x) \quad \text{(B3)}$$

where $\theta(x) = 1$ for $x > 0$, and 0 otherwise. Spatial distributions in this phase are determined by the interplay between motor transport at velocities $\pm v$ and the Poisson statistics of kinetically determined detachment and rebinding.

In the intermediate phase, all propagators are confined to the region $|x| < vt$ of motor transport as expected, but each propagator has a characteristic spatial distribution (Fig. 14). The following statements derive from Eqs. B3, and can be checked against the distributions in Fig. 11 by summing over final states. For duty ratios >0.5, the second term of $G_{oo}(x, t)$ shows two peaks, at $x = \pm v[t - 1/(2k - k')]$, which move out from the origin at the motor speed v after a time delay. The sharpness of these peaks increases as k' is reduced but their height, equal to $[2kk'/(2k - k')v]\exp(-k't - 1)$, decreases. As a function of time, the peaks are highest at the time of onset. G_{+o} is confined to positive displacements and peaks at $x = vt$ with height $(k/v)\exp(-k't)$, the sharpness of the peak behaving in the same way; in this case there is no delay time as binding proceeds from the outset. G_{-+} is a symmetric function of x; the kinetics of detachment and rebinding give the vesicle an equal chance of spending longer time on either track. This distribution is peaked at $x = 0$, but the maximum is very shallow when $K \gg 1$, giving a flat plateau within the propagation region. The height at $x = 0$ is equal to

$$\frac{kk'}{2(2k - k')v}(e^{-k't} - e^{-2kt}) \quad \text{(B4)}$$

which takes its maximum value when $t = \ln(2K)/(2k - k')$. When $K \gg 1$, this time can be somewhat longer than the onset times for other propaga-

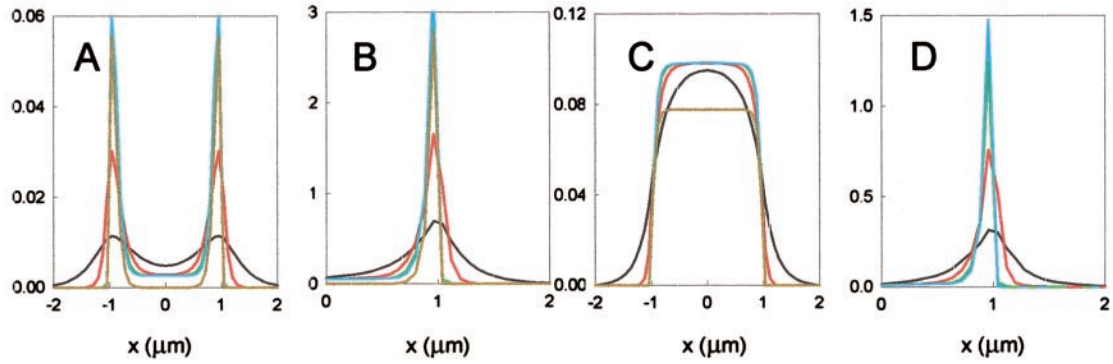

FIGURE 14 Sequences of the propagators $G_{oo}(x, t)(A)$, $G_{+o}(x, t)(B)$, $G_{-+}(x, t)(C)$, and $G_{++}(x, t)(D)$ against displacement x after 5 s, computed for decreasing values $D = 0.1$ (*black lines*), 0.01 (*red lines*), 0.001 (*green lines*), and 10^{-10} $\mu m^2/s$ (*blue lines*) of the diffusion constant, to be compared with "first-cycle" formulae (B3) valid for $D = 0$ (*khaki lines*). The distributions converge correctly for $D < 0.01$ $\mu m^2/s$, except for G_{-+}, where the distribution does not decay during the intermediate phase, and higher-order terms in the expansion in cycles are required.

tors. G_{++} is also confined to positive x because the restriction to one cycle forbids binding to the negative track; the distribution is localized near the motor edge $x = vt$ with a peak value $(kk't/v)\exp(-k't)$, which is maximal in time when $t = 1/k'$. In this case the intermediate phase is much prolonged when $k' \ll k$.

The distributions (B3) are qualitatively reproduced by numerical solution of Eqs. 1 using direct integration or Fourier methods for $D < 0.01$ $\mu m^2/s$, with other parameters as in Table 1. Fig. 14 shows the extent of agreement at a fixed time within the intermediate phase; the only serious discrepancy is for G_{-+}, where the height of the plateau from Eq. B4 is 20% smaller than the true distribution, the discrepancy becoming bigger with time. However, the spatial shapes of all distributions in the intermediate time domain are remarkably well-predicted by the one-cycle terms in the expansion of Eqs. B1.

We thank Dr. Dennis Bray for his helpful comments on the manuscript. D.A.S. is supported by a project grant from the Wellcome Trust.

REFERENCES

Adams, R. J., and D. Bray. 1983. Rapid transport of foreign particles microinjected into crab axons. *Nature.* 303:718–720.

Allen, R. D., J. Metuzals, I. Tasaki, S. T. Brady, and S. P. Gilbert. 1982. Fast axonal transport in squid giant axon. *Science.* 218:1127–1128.

Baas, P. W., and W. Yu. 1998. A composite model for establishing the microtubule arrays of the neuron. *Mol. Neurobiol.* 12:145–161.

Breuer, A. C., P. M. Eagles, M. P. Lynn, M. B. Atkinson, S. P. Gilbert, L. Weber, J. Leatherman, and J. M. Hopkins. 1988. Long-term analysis of organelle translocation in isolated axoplasm of *Myxicola infundibulum. Cell Motil. Cytoskeleton.* 10:391–399.

Bridgman, P. C. 1999. Myosin Va movements in normal and dilute-lethal axons provide support for a dual filament motor complex. *J. Cell Biol.* 146:1045–1060.

Buchner, K., D. Seitz-Tutter, K. Schonitzer, and D. G. Weiss. 1987. A quantitative study of anterograde and retrograde axonal transport of exogenous proteins in olfactory nerve C-fibres. *Neuroscience.* 22: 697–707.

Cann, J. R. 1970. Interacting Macromolecules. Academic Press, New York and London.

Carslaw, H. S., and J. C. Jaeger. 1959. Conduction of Heat in Solids, 2nd Ed. Clarendon Press, Oxford.

Chandrasekhar, S. 1943. Stochastic problems in physics and astronomy. *Rev. Mod. Phys.* 15:1–43.

Cheney, R. E., M. K. O'Shea, J. E. Heuser, M. V. Coelho, J. S. Wolenski, E. M. Espreafico, P. Forscher, R. E. Larsen, and M. S. Mooseker. 1993. Brain myosin-V is a two-headed unconventional myosin with motor activity. *Cell.* 75:13–23.

Cooper, P. D., and R. S. Smith. 1974. The movement of optically detectable organelles in myelinated axons of *Xenopus laevis. J. Physiol.* 242:77–97.

Cramer, L. P. 1997. Molecular mechanism of actin-dependent retrograde flow in lamellipodia of motile cells. *Frontiers in Bioscience.* 2:260–270.

Dayel, M. J., E. F. Y. Horn, and A. S. Verkman. 1999. Diffusion of green fluorescent protein in the aqueous-phase lumen of endoplasmic reticulum. *Biophys. J.* 76:2843–2851.

de la Cruz, E. M., A. L. Wells, S. S. Rosenfeld, E. M. Ostap, and H. L. Sweeney. 1999. The kinetic mechanism of myosin V. *Proc. Natl. Acad. Sci. USA.* 96:13726–13731.

Evans, L. L., and P. C. Bridgman. 1995. Particles move along actin filament bundles in nerve growth cones. *Proc. Natl. Acad. Sci. USA.* 92:10954–10958.

Evans, L. L., A. J. Lee, P. C. Bridgman, and M. S. Mooseker. 1998. Vesicle-associated brain myosin-V can be activated to catalyse actin-based transport. *J. Cell Sci.* 111:2055–2066.

Galbraith, J. A., T. S. Reese, M. L. Schlieff, and P. E. Gallant. 1999. Slow transport of unpolymerized tubulin and polymerized neurofilament in the squid giant axon. *Proc. Natl. Acad. Sci. USA.* 96:11589–11594.

Gilbert, G. A., and R. C. L. Jenkins. 1959. Sedimentation and electrophoresis of interacting substances II. Asymptotic boundary shape for two substances interacting reversibly. *Proc. R. Soc. (Lond.) A.* 250:420–437.

Hackney, D. 1995. Highly processive microtubule-stimulated ATP hydrolysis by dimeric kinesin head domains. *Nature.* 377:448–450.

Hannon, R., E. G. Richards, and H. J. Gould. 1986. Facilitated diffusion of a DNA binding protein on chromatin. *EMBO J.* 5:3313–3319.

Hayden, J. H., R. D. Allen, and R. D. Goldman. 1983. Cytoplasmic transport in keratocytes: direct visualization of particle translocation along microtubules. *Cell Motil.* 3:1–19.

Heidemann, S. R., M. A. Hamborg, S. J. Thomas, B. Song, S. Lindley, and D. Chu. 1984. Spatial organization of axonal microtubules. *J. Cell Biol.* 99:1289–1295.

Heidemann, S. R., J. M. Landers, and M. A. Hamborg. 1981. Polarity orientation of axonal microtubules. *J. Cell Biol.* 91:661–665.

Hou, L., F. Lanni, and K. Luby-Phelps. 1990. Tracer diffusion in F-actin and Fi-coll mixtures. Toward a model for cytoplasm. *Biophys. J.* 58: 31–43.

Janson, L. W., K. Ragsdale, and K. Luby-Phelps. 1996. Mechanism and size cut-off for steric exclusion from actin-rich cytoplasmic domains. *Biophys. J.* 71:1228–1234.

Jimbow, K., and S. Sugiyama. 1998. Melanosomal translocation and transfer. *In* The Pigmentary System: Physiology and Pathophysiology. J. J. Nordlund, R. E. Boissy, V. J. Hearing, R. King, and J-P. Ortonne, editors. Oxford University Press. 107–114.

Kelleher, J. F., and M. A. Titus. 1998. Intracellular motility: how can we all work together? *Curr. Biol.* 8:R394–R397.

Koles, Z. J., K. D. McLeod, and R. S. Smith. 1982. A study of the motion of organelles which undergo retrograde and anterograde rapid axonal transport in *Xenopus*. *J. Physiol.* 328:469–484.

Kuznetsov, S. A., G. M. Langford, and D. G. Weiss. 1992. Actin-dependent organelle movement in squid axoplasm. *Nature.* 356: 722–725.

Kuznetsov, S. A., D. T. Rivera, F. F. Severin, D. G. Weiss, and G. M. Langford. 1994. Movement of axoplasmic organelles on actin filaments from skeletal muscle. *Cell Motil. Cytoskeleton.* 28:231–242.

Lambert, J., G. Vancoillie, and J. M. Naeyaert. 1999. Molecular motors and their role in pigmentation. *Cell. Mol. Biol.* 45:905–918.

Langford, G. M. 1995. Actin- and microtubule-dependent organelle motors: interrelationships between the two motility systems. *Curr. Biol.* 7:82–88.

McQuarrie, D. M. 1962. Statistical Mechanics. Harper and Row, New York.

Mehta, A. D., R. S. Rock, M. Rief, J. A. Spudich, M. S. Mooseker, and R. E. Cheney. 1999. Myosin-V is a processive actin-based motor. *Nature.* 400:590–593.

Morris, R. L., and P. J. Hollenbeck. 1995. Axonal transport of mitochondria along microtubules and F-actin in living vertebrate neurons. *J. Cell Biol.* 131:1315–1326.

Olveczky, B. P., and A. S. Verkman. 1998. Monte Carlo analysis of obstructed diffusion in three dimensions: application to molecular diffusion in organelles. *Biophys. J.* 74:2722–2730.

Press, W. H., S. A. Teukolsky, W. T. Vetterling, and B. A. Flannery. 1992. Numerical Recipes in Fortran, 2nd Ed. Cambridge University Press.

Provance, D. W., A. McDowall, M. Marko, and K. Luby-Phelps. 1993. Cytoarchitecture of size-excluding compartments in living cells. *J. Cell Sci.* 106:565–578.

Provance, D. W., M. Wei, V. Ipe, and J. A. Mercer. 1996. Cultured melanocytes from dilute mutant mice exhibit dendritic morphology and altered melanosome distribution. *Proc. Natl. Acad. Sci. USA.* 93: 14554–14558.

Rebhun, L. I. 1963. Saltatory particle movements and mitosis. *In* The Cell in Mitosis. L. Levine, editor. Academic Press, New York. 67–103.

Rodionov, V. I., A. J. Hope, T. M. Svitkina, and G. G. Borisy. 1998. Functional coordination of microtubule-based and actin-based motility in melanophores. *Curr. Biol.* 8:165–168.

Rogers, S. L., I. S. Tint, P. C. Fanapour, and V. I. Gelfand. 1997. Regulated bidirectional motility of melanophore pigment granules along microtubules in vitro. *Proc. Natl. Acad. Sci. USA.* 94:3720–3725.

Rogers, S. L., and V. I. Gelfand. 1998. Myosin cooperates with microtubule motors during organelle transport in melanophores. *Curr. Biol.* 8:161–164.

Schliwa, M., K. Weber, and K. R. Porter. 1981. Localization and organization of actin in melanophores. *J. Cell Biol.* 89:267–275.

Schnapp, B. J., and T. D. Reese. 1989. Dynein is the motor for retrograde axonal transport of organelles. *Proc. Natl. Acad. Sci. USA.* 86: 1458–1552.

Schnapp, B. J., R. D. Vale, M. P. Sheetz, and T. D. Reese. 1985. Single microtubules from squid axoplasm support bidirectional movement of organelles. *Cell.* 40:455–462.

Schroer, T. A., E. R. Steuer, and M. P. Sheetz. 1989. Cytoplasmic dynein is a minus end-directed motor for membranous organelles. *Cell.* 56: 937–946.

Sheetz, M. P., and J. A. Spudich. 1983. Movement of myosin-coated fluorescent beads on actin cables in vitro. *Nature.* 303:31–35.

Svoboda, K., and S. M. Block. 1994. Force and velocity measured for single kinesin molecules. *Cell.* 77:773–784.

Svoboda, K., P. P. Mitra, and S. M. Block. 1994. Fluctuation analysis of motor protein movement and single enzyme kinetics. *Proc. Natl. Acad. Sci. USA.* 91:11782–11786.

Svoboda, K., C. F. Schmidt, B. J. Schnapp, and S. M. Block. 1993. Direct observation of kinesin stepping by optical trapping interferometry. *Nature.* 365:721–727.

Tabb, J. S., B. J. Molyneaux, D. L. Cohen, S. A. Kuznetsov, and G. M. Langford. 1998. Transport of ER vesicles on actin filaments in neurons by myosin V. *J. Cell Sci.* 111:3221–3234.

Vale, R. D., T. S. Reese, and M. P. Sheetz. 1985a. Identification of a novel force-generating protein, kinesin, involved in microtubule-based motility. *Cell.* 42:39–50.

Vale, R. D., B. J. Schnapp, T. S. Reese, and M. P. Sheetz. 1985b. Movement of organelles along filaments dissociated from the axoplasm of the squid giant axon. *Cell.* 40:449–454.

van Holde, K. E. 1962. Sedimentation in chemically reacting systems. I. The isomerization reaction. *J. Chem. Phys.* 37:1922–1926.

Wei, Q., X. Wu, and J. A. Hammer III. 1997. The predominant defect in dilute melanocytes is in melanosome distribution and not cell shape, supporting a role for myosin V in melanosome transport. *J. Muscle Res. Cell Motil.* 18:517–527.

Weiss, D. G., F. Keller, J. Gulden, and W. Maile. 1986. Towards a new classification of intracellular particle movements based on quantitative analysis. *Cell Motil. Cytoskeleton.* 6:128–135.

Winkelmann, D. A., L. Bourdieu, A. Ott, F. Kinose, and A. Libchaber. 1995. Flexibility of myosin attachment to surfaces influences F-actin motion. *Biophys. J.* 63:2444–2453.

Wittenberg, J. B. 1966. The molecular mechanism of hemoglobin-facilitated oxygen diffusion. *J. Biol. Chem.* 241:104–114.

Wittenberg, B. A., J. B. Wittenberg, and P. R. B. Caldwell. 1975. Role of myoglobin in the oxygen supply to red skeletal muscle. *J. Biol. Chem.* 250:9038–9043.

Wolenski, J. S., R. E. Cheney, M. S. Mooseker, and P. Forscher. 1995. In vitro motility of immunoadsorbed brain myosin-V using a *Limulus* acrosomal process and optical tweezer-based assay. *J. Cell Sci.* 108: 1489–1496.

Wu, X., B. Bowers, K. Rao, Q. Wei, and J. A. Hammer. 1998. Visualization of melanosome dynamics within wild-type and dilute melanocytes suggests a paradigm for myosin V function in vivo. *J. Cell Biol.* 143:1899–1918.

Wu, X., B. Bowers, Q. Wei, B. Kocher, and J. A. Hammer III. 1997. Myosin V associates with melanosomes in mouse melanocytes: evidence that myosin V is an organelle motor. *J. Cell Sci.* 110:847–859.

Wyman, J. 1966. Facilitated diffusion and the possible role of myoglobin as a transport mechanism. *J. Biol. Chem.* 241:115–121.